Available online at www.sciencedirect.com
ScienceDirect
International Journal of Mechanical Sciences 49 (2007) 533–553
International Journal of MECHANICAL SCIENCES
www.elsevier.com/locate/ijmecsci

Effects of the UOE/UOC pipe manufacturing processes on pipe collapse pressure

M.D. Herynk, S. Kyriakides*, A. Onoufriou, H.D. Yun

Research Center for Mechanics of Solids, Structures and Materials, WRW 110, C0600, The University of Texas at Austin, Austin, TX 78712, USA

Received 30 May 2006; received in revised form 10 October 2006; accepted 16 October 2006
Available online 8 December 2006

Abstract

Large-diameter pipes used in offshore applications are commonly manufactured by cold-forming plates through the UOE process. The plate is crimped along its edges, formed into a U-shape and then pressed into an O-shape between two semicircular dies. The pipe is welded closed and then circumferentially expanded to obtain a highly circular shape. Collapse experiments have demonstrated that these steps, especially the final expansion, degrade the mechanical properties of the pipe and result in a reduction in its collapse pressure upwards of 30%. In this study the UOE forming process has been modeled numerically using a 2-D finite element model. The model can assess the effects of press parameters of each forming step on the final geometry and mechanical properties of the pipe. The final step involves simulation of pipe collapse under external pressure in order to quantify the effect of the forming variables on its performance. Examples of these variables are the radii of the forming dies, the chosen displacements of the dies, the compression strain in the O-step, the expansion strain, etc. An extensive parametric study of the problem has been conducted, through which ways of optimizing the process for improved collapse performance have been established. For example, it was found that optimum collapse pressure requires a tradeoff between pipe shape (ovality) and material degradation. Generally, increase in the O-strain and decrease in the expansion strain improve the collapse pressure. Substituting the expansion with compression can not only alleviate the UOE collapse pressure degradation but can result in significant increases in collapse performance.

Keywords: UOE-pipe; UOC-pipe; Collapse pressure

1. Introduction

Pipes used to transport oil and gas larger than approximately 16 in in diameter are commonly manufactured by cold forming of 40–60 ft (12.2–18.3 m) long plates. The plates are formed into a circular cylindrical shape through the four mechanical steps shown schematically in Fig. 1. The plate edges are first crimped into circular arcs (Fig. 1a). The plate is then formed into a U-shape in the "U-press" (Fig. 1b). It is then pressed into a circular shape in the "O-press" (Fig. 1c). The seam is subsequently welded using submerged arc welding. In the final step the pipe is mechanically expanded (Fig. 1d) as a means of final sizing and improving its circularity. The name UOE stems from the initials of the last three of these mechanical steps.

UOE pipe has been widely used for land pipelines, including the Trans-Alaska and Trans-Siberia pipelines. In the last 15 years it has also been increasingly used in offshore applications where collapse under external pressure is a primary design consideration and, as a result, high circularity is required [1–3]. Modern UOE pipe mills are capable of delivering pipes of high circularity with typical ovality values ranging between 0.15% and 0.35%. Despite their low ovalities, experiments have demonstrated that the collapse pressure of such pipes can be significantly lower than that of corresponding seamless pipes. For typical pipe geometries and plate material properties, the degradation in collapse pressure of UOE pipe can exceed 30%.

The reasons behind this degradation in collapse pressure were first identified in Ref. [4]. It was demonstrated that the four cold-forming steps, in particular the final expansion, introduce changes to the compressive stress–strain response of the pipe in the circumferential direction. This is

*Corresponding author. Fax: +1 512 471 5500.
E-mail address: skk@mail.utexas.edu (S. Kyriakides).

0020-7403/$ - see front matter © 2006 Elsevier Ltd. All rights reserved.
doi:10.1016/j.ijmecsci.2006.10.001

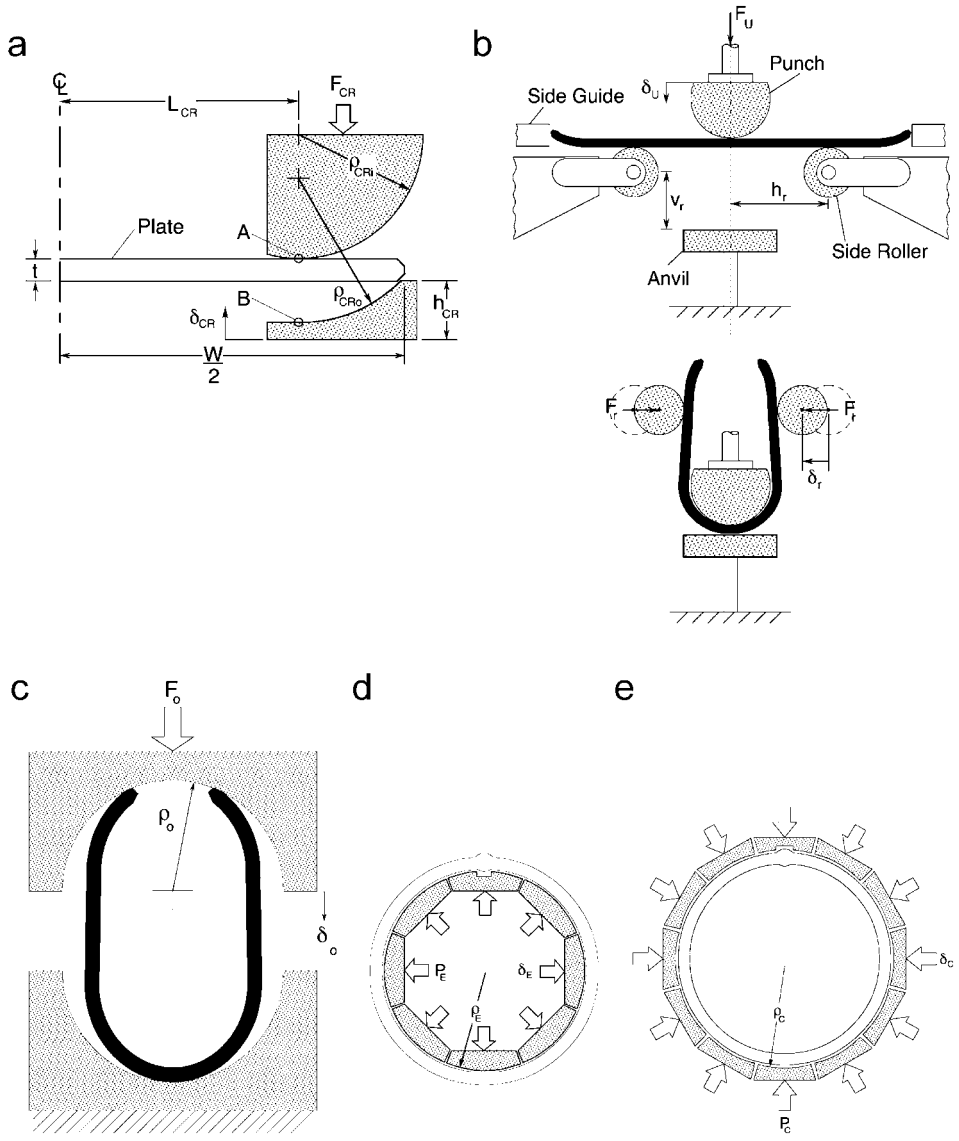

Fig. 1. Schematic and main parameters of UOE and UOC forming steps. (a) Crimping press, (b) U-press, (c) O-press, (d) expansion and (e) compression.

illustrated in Fig. 2 for a 24 in X-70 pipe with wall thickness of 1.273 in (32.33 mm). Compressive stress–strain responses from circumferential specimens extracted from two locations through the thickness, and the stress–strain response of the original plate are shown. The mechanical work has rounded the stress–strain responses significantly and lowered the stress in the critical strain range for collapse of 0.3–0.5%. The collapse pressure of the as-received pipe was calculated to be 5059 psi (348.9 bar). By contrast, when the same pipe geometry is assigned the plate mechanical properties, the collapse pressure becomes 7508 psi (517.8 bar), an increase of 48%.

This high level of degradation in collapse pressure was first demonstrated in full-scale tests performed in support of the Oman–India pipeline [5]. Eleven collapse tests were performed on 20 in pipe supplied by three different manufacturers (X65 nominal, $t = 1.125$ in—28.58 mm). Nine pipes were tested in the as-received state. Their collapse

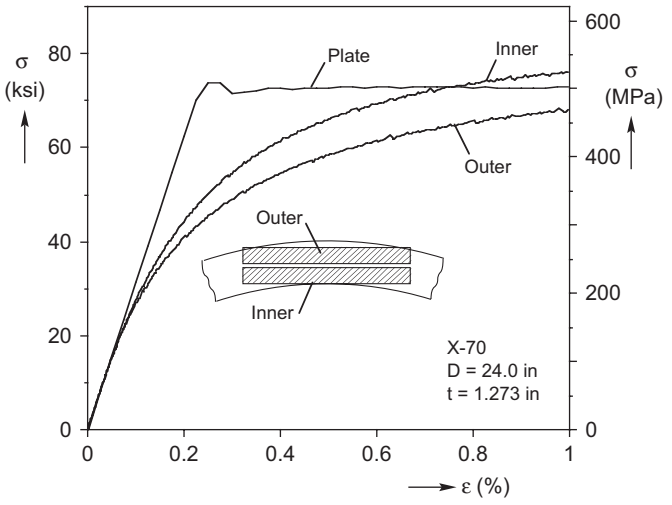

Fig. 2. Comparison of plate stress–strain response and responses from transverse UOE specimens tested in compression.

pressures ranged from 5270 to 6671 psi (363.4–460.1 bar), with an average value of 5815 psi (401.1 bar). Two of the pipes were heat-treated (normalizing temperature) so that the sharp yield point and Lüders banding behavior were retrieved and residual stresses erased. Their collapse pressures were 8429 psi (581.3 bar) and 8839 psi (609.6 bar). Thus, if we compare the average values of the collapse pressures of the two heat-treated pipes to the average value measured in the nine as-received pipes, we find that the UOE process resulted in a decrease of 33% in collapse pressure.

A 33% degradation in collapse pressure translates into a significantly higher wall thickness requirement (as much as 20% higher). This in turn results in higher material costs but also in higher offshore installation costs due to the increased line weight. In addition, there exist limits in the plate wall thickness that can be formed into pipe by modern pipe mills. These limits were, for example, challenged in the case of the Oman–India project were the pipeline was designed to cross waters as deep as 3350 m (11 000 ft). Thus, increase in the collapse pressure over current performance can be decisive, in that it directly affects the cost of the project but can also make some projects feasible.

One approach to the problem taken was to explore further the benefits of heat-treating the pipe. Full stress relieving is very costly and can have detrimental effects on the welds and on corrosion resistance. Subsequent work showed that a more modest heat treatment process involving heating to about 230 °C for a few minutes can recover the compressive yield stress leading to higher collapse pressure [6]. This recovery is caused by strain aging of the material. The elevated temperature allows interstitial solute atoms such as carbon and nitrogen to diffuse around dislocations, pinning them [7]. Many pipelines are coated with epoxies for corrosion protection. Several of these coatings are fusion bonded to the steel requiring that the pipe be heated to 225–250 °C for a short time (30–60 s). Thus strain aging can be a byproduct of the coating process. The potential benefits of the process on the collapse performance have been explored and proven in several recent testing programs (e.g. Refs. [8–10]).

Simultaneous to the exploration of the benefits of heat treatment, efforts were undertaken to better understand the effect of the four forming steps on the collapse performance of the pipe. Kyriakides et al. [4] developed a simple one-dimensional model of the forming process that was shown to capture the essence of the changes introduced to the compressive mechanical properties. Using this model it was demonstrated that for the most part, the expansion is responsible for the degradation. Indeed they suggested that if the final expansion step is replaced by compression, the pipe can reach performance levels that are higher than those of heat treatment.

The one-dimensional model of Ref. [4] does not capture variations of properties around the circumference or the final shape. This paper describes a more elaborate 2-D finite element model of the process that can accurately simulate each forming step. The finished pipe can then be collapsed under external pressure. The model will be used to develop an understanding of how each step influences the shape and mechanical properties as well as the collapse pressure. A parametric study of the process is used to show that significant improvements in collapse performance can be achieved by altering some of the forming parameters from accepted standards. In addition, the proposed alternative process where the final expansion is replaced with compression (UOC, [4]) is evaluated further.

2. The UOE process

The UOE process starts by trimming the longitudinal edges of the plate by milling, bringing the width to the exact required value. Simultaneously, the ends are beveled to later form v-grooves in the circular skelp to accommodate the welding. The first forming step involves crimping of the edges of the plate into circular arcs over a width of about one radius on each side. This is achieved by pressing the ends between two shaped dies as shown in Fig. 1a. Because of the large forces required, this is done in steps, involving lengths of one to four pipe diameters depending on the wall thickness. In order to accommodate different pipe thicknesses and diameters, several sets of dies are available. For a given pipe, the dies with the most appropriate inner and outer radii (ρ_{CRi} and ρ_{CRo}) are selected. The relative horizontal positions of the dies can be adjusted to accommodate for mismatch between the die radii and the thickness of the plate. The width of plate to be crimped, set by the horizontal placement of the dies (L_{CR}), can be influenced by the thickness of the plate and the load capacity of the press.

The plate moves next to the U-press, where it initially rests centered between a pair of side rollers that run along its entire length (Fig. 1b). The U-punch moves down and bends the entire plate through three-point bending. The radius of the punch ρ_U is selected so that the lower half of the plate acquires an outer radius near that of the final pipe (see Fig. 3a and b). The U-punch stops when the plate contacts a series of anvils set at a predetermined height. The U-punch is then held in place, and the side rollers are moved inwards as shown in Fig. 1b. The horizontal position (h_r) and inward travel (δ_r) of the rollers are selected such that the final position of the straight arms of the U-shaped plate or "skelp" are nearly vertical.

The skelp is then conveyed to the O-press, which consists of two semi-circular (radius ρ_O) stiff dies, as shown in Figs. 3b and 1c. The top die is actuated downwards, forcing the skelp into a nearly circular shape (Fig. 3c). The forming finishes by forcing the dies further together, producing a net compressive strain of 0.1–0.2%.

After leaving the O-press, the pipe seam is welded using submerged arc welding machines that weld it first on the inside and then on the outside. Extensive ultrasonic examination is performed on the weld before the pipe is expanded.

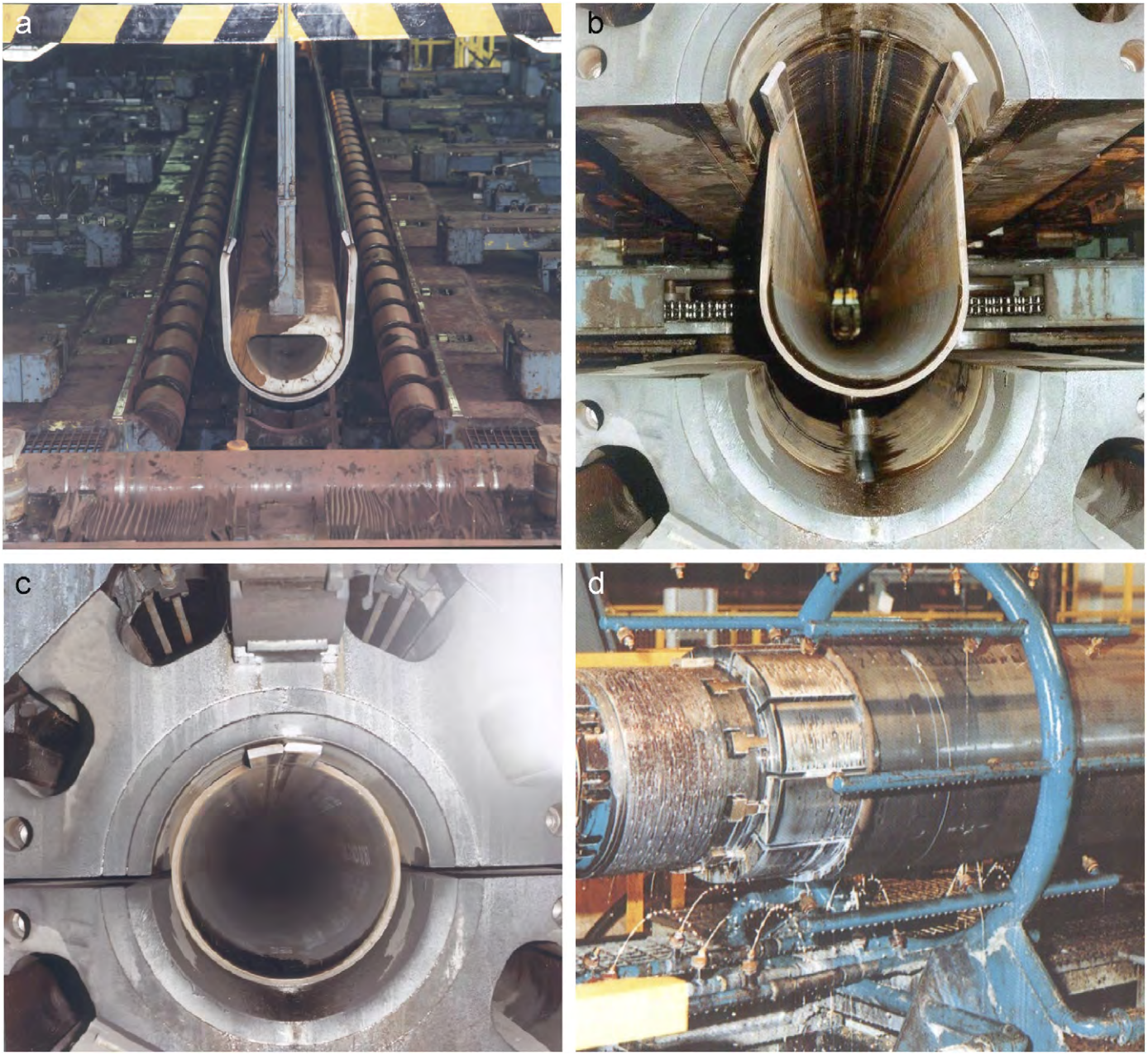

Fig. 3. Photographs of (a) the U-press, (b) and (c) the O-press, and (d) the pipe expander. (Courtesy, Corus Tubes, UK).

Expansion is accomplished by an internal mandrel, shown in Figs. 3d and 1d. The mandrel consists of 8, 10, or 12 segments. Segments are chosen so that their radii (ρ_E) are near that of the inside of the pipe. The mandrel is hydraulically actuated, and in one step it typically expands a length of one half to one diameter (depending on the wall thickness). Each step maintains some overlap between the expanded and unexpanded pipe sections. Expansion improves the roundness of the pipe and brings it to its desired final size. To achieve low ovality, the pipe is typically expanded 0.8–1.3% from its diameter after the O-step.

Compressive devices that would substitute the expanders do not exist for large-diameter pipes. A small number of such devices exist for smaller pipes made by the ERW process (US Patent 2,999,405 by Ewart, 1961 [11]). Fig. 1e shows a schematic of such a device with twelve mandrel segments with radius ρ_C. It is envisioned to operate in a fashion similar to that of the expanders.

3. Numerical simulation of UOE process

3.1. Discretization

All forming steps are assumed to take place under plane strain conditions. In addition, symmetry about the plate mid-width is assumed. The problem is solved within the nonlinear FE code ABAQUS using a user-defined

nonlinear kinematic hardening plasticity subroutine. The structure is discretized by linear, reduced integration plane strain continuum elements (CPE4R). Fig. 4 shows the mesh adopted after convergence studies. There are 7 elements through the thickness. Along the length there are 110 elements in the main part of the plate (W_1), 10 elements in the edge of the straight part (W_2), and 15 elements in the section beveled to accommodate welding (W_3). The plate geometry is altered by prescribing new values of for W, W_i, t, and t_i.

All forming dies were modeled as analytical rigid surfaces, whereas the plate is deformable. The plate surface is defined as three surfaces covering its perimeter: the top surface, the bottom surface, and the surface of the three-faced bevel. ABAQUS defines the contact between two surfaces using a strict "master–slave" algorithm. Rigid surfaces constitute the master surface in a contact pair. The contact pairs are allowed "finite sliding," while contact was assumed to be frictionless. The "soft" option was adopted with $p^o = 10\,000$ psi (69 MPa) and $c = 0.005$ in (0.127 mm) being representative pressure and clearance values used. One contact pair, that between the U-punch and the top of the plate, was defined using "no-separation" contact instead of soft contact to avoid relative motion between the two. This was done to prevent the plate from slipping off the U-punch as it is pushed down. In this contact scheme, the nodes of the slave surface are not allowed to move normal to the surface, but they can still slide on the surface.

3.2. Constitutive model

The pipe material undergoes elastic–plastic deformations that include load reversals. These challenges were addressed using the two-surface nonlinear kinematic hardening model of Dafalias and Popov [12,13]. A unique feature of the model is the method used to evaluate the plastic modulus. In the uniaxial setting, represented in Fig. 5a by the stable hysteresis bcde, the plastic modulus of point d depends on the stress variables δ and δ_{in}. Both are distances measured from line XY, called *the bound*, which

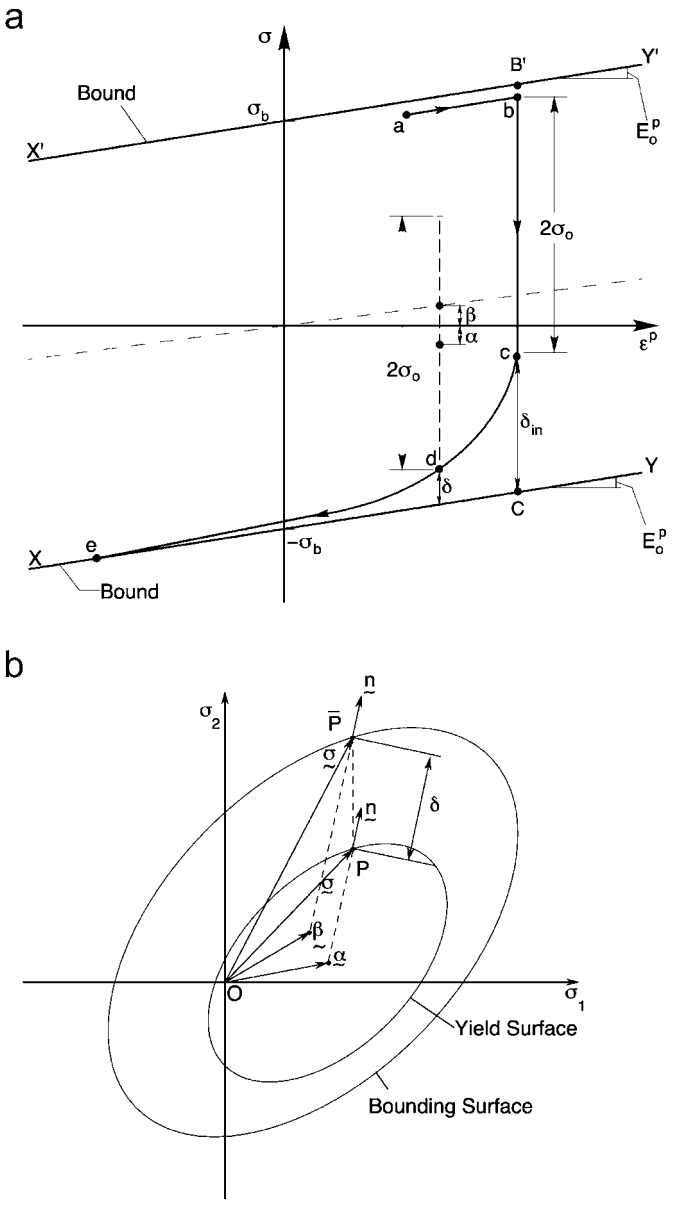

Fig. 5. (a) The uniaxial stress–strain variables in the Dafalias–Popov model. (b) The yield and bounding surfaces and associated variables in the Dafalias–Popov model.

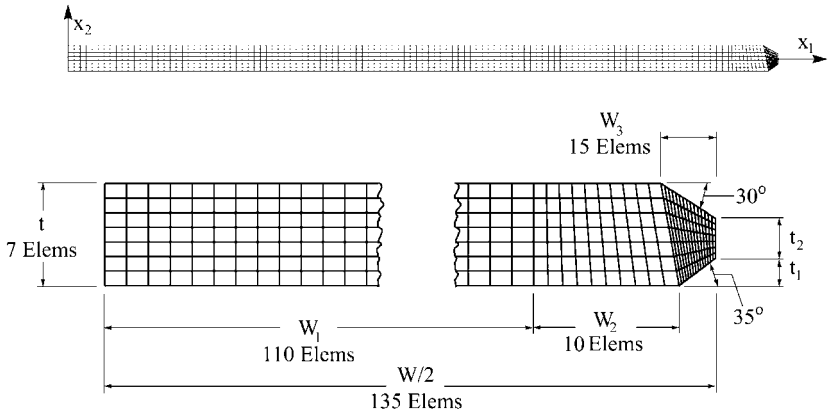

Fig. 4. The finite element mesh of UOE model.

is the tangent to the stress-plastic strain response at a large value of strain (point e in this case). Thus, δ is the distance of point d from the bound and δ_{in} is the distance of the last elastic state, point c, from the same line. The plastic modulus H is related to these variables as follows:

$$H(\delta,\delta_{in}) = E_o^p + h\left(\frac{\delta}{\delta_{in}-\delta}\right), \tag{1}$$

where E_o^p is the modulus of the bound and h is a calibration constant which, in the simplest case, is evaluated through a one-point fit of an experimental stress–strain response. A second bounding line X′Y′ is drawn parallel to XY as shown in the figure.

In the multiaxial setting the YS bc is represented as follows:

$$f(\boldsymbol{\sigma}-\boldsymbol{\alpha}) = \left[\frac{3}{2}(\boldsymbol{s}-\boldsymbol{a})\cdot(\boldsymbol{s}-\boldsymbol{a})\right]^{1/2} = \sigma_o, \tag{2}$$

where $\boldsymbol{\sigma}$ is the stress tensor and $\boldsymbol{\alpha}$ is the center of the yield surface in stress space; $\boldsymbol{s}$ and $\boldsymbol{a}$ are the respective deviatoric tensors and σ_o is the size of the yield surface assumed to remain constant. B′C becomes a *bounding surface* (BS) that encloses the YS, and is defined by

$$F(\bar{\boldsymbol{\sigma}}-\boldsymbol{\beta}) = \left[\frac{3}{2}(\bar{\boldsymbol{s}}-\boldsymbol{b})\cdot(\bar{\boldsymbol{s}}-\boldsymbol{b})\right]^{1/2} = \sigma_b. \tag{3a}$$

Here, σ_b is the size of the BS, $\bar{\boldsymbol{\sigma}}$ is the congruent point on the BS to $\boldsymbol{\sigma}$ on the YS, $\boldsymbol{\beta}$ is the center of the BS, and $\bar{\boldsymbol{s}}$ and $\boldsymbol{b}$ are, respectively, their deviators. The two surfaces are geometrically similar, and as a result, points P and $\bar{\text{P}}$ are congruent when they have the same normals, as shown in Fig. 5b. Thus, the two points are related through

$$(\bar{\boldsymbol{\sigma}}-\boldsymbol{\beta}) = \frac{\sigma_b}{\sigma_o}(\boldsymbol{\sigma}-\boldsymbol{\alpha}). \tag{3b}$$

The scalar δ is generalized as follows (see Fig. 5b):

$$\delta = [(\bar{\boldsymbol{\sigma}}-\boldsymbol{\sigma})\cdot(\bar{\boldsymbol{\sigma}}-\boldsymbol{\sigma})]^{1/2}. \tag{4}$$

Evolution of the yield surface and bounding surface: The YS translates in stress space according to a chosen hardening rule that in general is defined by

$$\mathrm{d}\boldsymbol{\alpha} = \mathrm{d}\mu\boldsymbol{v}, \quad \boldsymbol{v}\cdot\boldsymbol{v} = 1. \tag{5}$$

The amount of translation $\mathrm{d}\mu$ is chosen so that the consistency condition is satisfied. The YS translates along the direction $\text{P}\bar{\text{P}}$ in Fig. 5b given by

$$v_{ij} = \frac{(\bar{\sigma}_{ij}-\sigma_{ij})}{|\bar{\sigma}_{ij}-\sigma_{ij}|}. \tag{6}$$

Here $\bar{\boldsymbol{\sigma}}$ is the image of $\boldsymbol{\sigma}$ on the outer surface [14]. The rule ensures that the two surfaces come into contact tangentially.

The translation of the BS is coupled to that of the YS as follows:

$$\mathrm{d}\beta_{ij} = \mathrm{d}\alpha_{ij} - \mathrm{d}M m_{ij}, \tag{7a}$$

where

$$m_{ij} = \frac{(\bar{\sigma}_{ij}-\sigma_{ij})}{|\bar{\sigma}_{ij}-\sigma_{ij}|}, \tag{7b}$$

and

$$\mathrm{d}M = \left(1-\frac{E_o^p}{H}\right)\left(\frac{\mathrm{d}\sigma_{ij}n_{ij}}{m_{kl}n_{kl}}\right). \tag{7c}$$

$\boldsymbol{n}$ in Eq. (7c) is the unit normal to the YS at the current stress point. When the two surfaces come into contact, the BS becomes the active surface and the YS moves so as to remain tangential to it.

The model was calibrated on a uniaxial stress–strain response obtained from a nominal X-70 plate material shown in Fig. 6. The response includes loading to about 7.6% strain, followed by unloading and reverse loading. The response exhibits Lüders banding behavior that extends to about 4.7%. Subsequently the material hardens and deforms uniformly. Reverse loading exhibits the Bauschinger effect.

The monotonic and hysteresis responses are modeled independently. The model parameters for each are given in Table 1. For numerical expediency, the Lüders banding is avoided by assigning a small positive constant slope to the monotonic part of the response. The fits of the two parts are drawn in Fig. 6 with a dashed line.

3.3. Collapse under external pressure

Once the forming is completed, the pipe is loaded by external pressure up to collapse. The pressurization is achieved by surrounding the pipe (one half of the cross section) with a fluid-filled cavity made of two-noded hydrostatic fluid elements (F2D2). Fluid is pumped into the cavity by using the cavity reference node as an inlet. This volume-controlled loading enables the tracing of the pressure maximum that corresponds to the collapse pressure (P_{CO}).

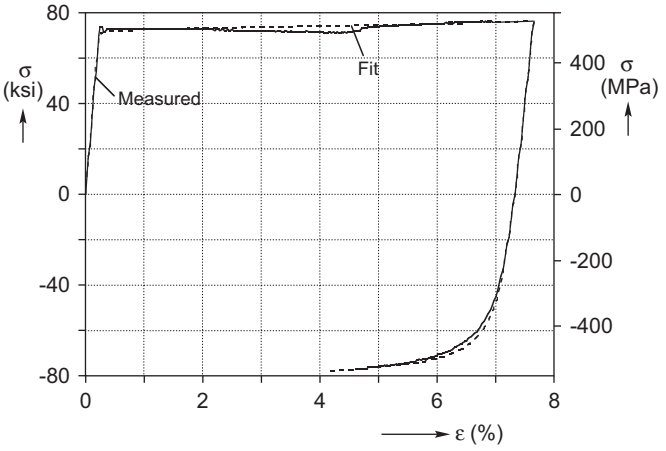

Fig. 6. Uniaxial plate stress–strain response and the Dafalias–Popov fit used in the simulation.

Table 1
Constitutive model parameters for base case

Part	E Msi (GPa)	v	σ_o ksi (MPa)	σ_b ksi (MPa)	E_o^P ksi (MPa)	h Msi (GPa)
Monotonic	31 (214)	0.3	68.0 (469)	72.14 (498)	55.8 (385)	5.0 (34.5)
Hysteresis	24 (165)	0.3	52.9 (365)	86.40 (596)	189 (1303)	10 (69)

4. Results

4.1. Base case forming

The capability of the model will be demonstrated using a "base case" example, consisting of a 24 in pipe with a wall thickness of 1.273 in (32.33 mm) and the mechanical properties given in Table 1. The process forming parameters used are listed in Table 2. These values are representative of those that a modern steel mill might use for this pipe. With these die parameters and a full closure of the O-dies, the net hoop strain in the pipe after the O-press is $\varepsilon_O = -0.205$, while the final expansion strain is $\varepsilon_E = 0.984\%$.

4.1.1. Crimping press

The crimping dies are modeled as circular arcs with inner and outer radii of ρ_{CRi} and ρ_{Cro}, respectively. Crimping is achieved by moving the outer die upwards (displacement δ_{CR}), while the inner one is stationary. The die is displaced until points A and B in Fig. 1a are a distance of $(t + 0.02)$ in apart, as illustrated in the sequence of configurations shown in Fig. 7. Fig. 8a shows the vertical force on the dies per unit length of plate (F_{CR}) versus δ_{CR}. During most of the crimping process (configuration ① in Fig. 7) the reaction force is nearly constant, but it ramps up sharply once the plate contacts the dies in a significant manner (configuration ② in Fig. 7). The added gap of 0.020 in (0.5 mm) ensures that reaction forces will not become excessive. At the end, the dies are moved apart and the plate springs back elastically.

4.1.2. U-press

A schematic of the U-process is shown in Fig. 1b and a set of calculated deformed configurations are included in Fig. 9. The roller analytical rigid surface is modeled as a circular segment with a radius of 5.0 in (127 mm), and its center is located h_r from the center of the plate. The U-punch is modeled as a circular arc with a radius of ρ_U. The anvil that supports the pipe once it is formed is represented as a rigid surface located a distance v_r below the center of the rollers. Soft contact is used for the rollers, while no-separation contact is used for the punch in order to prevent the plate from slipping off the punch before the anvil is contacted. In the first step, the U-punch moves down (δ_U) until the skelp contacts the anvil (see configurations ⓪ to ② in Fig. 9). The vertical force that develops per unit length of plate (F_U) is plotted against δ_U in Fig. 8b. The load reaches a maximum at about half of the total displacement, and then gradually drops as the plate continues to bend. The punch force is relatively low in this step because of the large moment arms involved. Next the rollers move inward a distance δ_r, bending the plate "arms" usually past vertical (configuration ③ in Fig. 9). The force on the rollers F_r per unit plate length is plotted against δ_r in Fig. 8c. The rollers are then retracted and the plate springs back to its final U-shape, with the "arms" nearly vertical (④ in Fig. 9).

4.1.3. O-press

The O-press is shown schematically in Fig. 1c, and three of its deformed configurations are shown in Fig. 10. The two dies are modeled as 90° circular arcs with radii ρ_O. The top die has a vertical segment at its crest that prevents the plate from crossing the symmetry line (see configuration ⓪). The upper die is moved down forcing the skelp to gradually conform to the circular shape (configuration ①). This step has high nonlinearity due to the plate coming in and out of contact as it bends, and extensive sliding contact of the plate edge on the top die. Fig. 8d depicts the vertical force per unit length (F_O) versus the die displacement δ_O. Displacement is measured from the point where the top die first touches the edges of the skelp. Before point a, the lower part of the skelp bends to match the curvature of the lower die. The top edges of the skelp then slide along the top die until they meet at point b. Beyond this point the skelp arms bend to match the curvature of the top die, and as a result the force rises. After point c, the resistance to bending decreases. At point d, the pipe essentially matches the shape of the dies, and further displacement compresses the pipe circumferentially. This results in the very stiff response seen after point d, as the dies come to full closure (configuration ②). Compression is terminated when the centers of the two half dies become coincident. Because in this press the whole length of pipe is formed at once, the force required is very significant indeed. Often this ends up being the step that defines the capacity of a given pipe mill. For this case, the pipe is compressed to $\varepsilon_{O1} = -0.288\%$, and unloads to a final value of $\varepsilon_O = -0.205\%$ after the dies are released.

4.1.4. Welding

In practice, after the O-step, the pipe is welded using submerged arc welding. This is an important step that is given immense attention in the mill, including manual, ultrasonic and radiographic inspections over the whole length of the seam. In the simulation, welding is modeled by replacing the elements in the beveled end with elements

Table 2
Parameters of the base case UOE simulation

	Variable	Description	Value
Plate	t	Thickness of the plate (in—mm)	1.273 (32.33)
	W	Width of the plate (in—mm)	71.00 (1803)
	X	Grade of the plate steel (ksi—MPa)	70 (482)
Crimp	ρ_{CRi}	Inner crimping radius (in—mm)	10.45 (265.4)
	ρ_{CRo}	Outer crimping radius (in—mm)	11.75 (298.5)
	δ_{CR}	Under-closure of crimp die (in—mm)	0.02 (0.5)[a]
	L_{CR}	Horizontal position of the dies (in—mm)	26.64 (676.7)
	h_{CR}	Height of outer crimp die (in—mm)	3.50 (88.9)[a]
U	ρ_U	Radius of U punch (in—mm)	9.70 (246.4)
	δ_U	U punch vertical travel (in—mm)	28.5 (724)
	δ_r	U roller horizontal travel (in—mm)	4.00 (102)
	h_r	Horizontal position of the roller (in—mm)	18.0 (457)[a]
	v_r	Vertical position of anvil (in—mm)	28.5 (724)
O	ρ_O	Radii of the O dies (in—mm)	11.959 (303.8)[a]
	δ_O	Overlap of the O dies' centers (in—mm)	0.00
E	ρ_E	Radii of the expansion mandrels (in—mm)	10.66 (270.8)
	δ_E	Radial expansion of mandrels (in—mm)	0.14 (3.6)
	N_E	Number of expansion mandrels	8
C	ρ_C	Radii of compression mandrels (in—mm)	11.88 (301.8)[a]
	δ_C	Radial compression of mandrels (in—mm)	0.14 (3.6)
	N_C	Number of compression mandrels	12[a]

[a]Indicates constant values.

without the bevel that are initially stress free. The end to which these elements are added is held fixed as this is done. When the replacement is completed, the constraint is removed and the new elements share whatever stress existed in the pipe.

4.1.5. Expansion

The expander used had 8 segments of radius ρ_E as shown in Fig. 1d. The rigid body reference nodes of the segments are located at the centers of the arcs. The expansion mandrel is first contracted slightly (0.50 in—12.7 mm) from the initial radius ρ_E so that it fits inside of the pipe. Expansion is accomplished by moving the reference nodes out radially a distance δ_E (configuration ① in Fig. 11). Rather than the force on each segment, we choose to monitor the equivalent pressure (P_E), defined as

$$P_E = \frac{1}{C}\sum_{n=1}^{N_E} F_E, \tag{8}$$

where F_E is the reaction force on an individual mandrel segment, N_E is the number of segments, and C is the circumference of the mandrel. At first, only the bottom mandrel is in contact with the pipe. Fig. 12a shows P_E vs. the applied displacement δ_E. Zero displacement is defined as the point where reaction forces are first detected. At approximately 0.15 in, all mandrels have contacted the pipe (point a). The pressure then rises sharply as the pipe expands and plasticizes. At point b, the whole cross section has been plasticized, and the expansion pressure subsequently increases at a lower rate. The final displacement is $\delta_E = 0.39$ in (9.9 mm). An alternative plot is given in Fig. 12b, where P_E is plotted against the average circumferential permanent strain ε_E, calculated as follows:

$$\varepsilon_E = \frac{C_E - C_O}{C_O}, \tag{9}$$

where C_E and C_O are, respectively, the mid-surface circumferences after E and O. In this case, the pipe is expanded to $\varepsilon_{E1} = 1.389\%$ and relaxes to $\varepsilon_E = 0.984\%$ on unloading.

4.1.6. Compression

In the model, compression is applied in place of expansion using a 12-segment mandrel with a radius $\rho_C = 11.88$ in (301.8 mm—see Fig. 1e). The compression mandrels are modeled in a manner similar to the expansion ones. The radial displacement of the mandrels δ_C (measured from the position when reaction forces are first detected) is prescribed. This results in the equivalent pressure–displacement (P_C–δ_C) response shown in Fig. 12c (P_C definition is similar to that of P_E; configurations shown in Fig. 13). The initial nonlinearity in the response (before point a) is due to increasing contact between the pipe and the mandrel. Between points a and b, the pipe conforms to the curvature of the mandrel. Beyond point b, the pipe is undergoing membrane compression. The final displacement is $\delta_C = 0.14$ in (3.56 mm). Fig. 12d shows a plot of P_C against the permanent compressive strain ε_C (calculated similar to ε_E in Eq. (11)). The pipe is

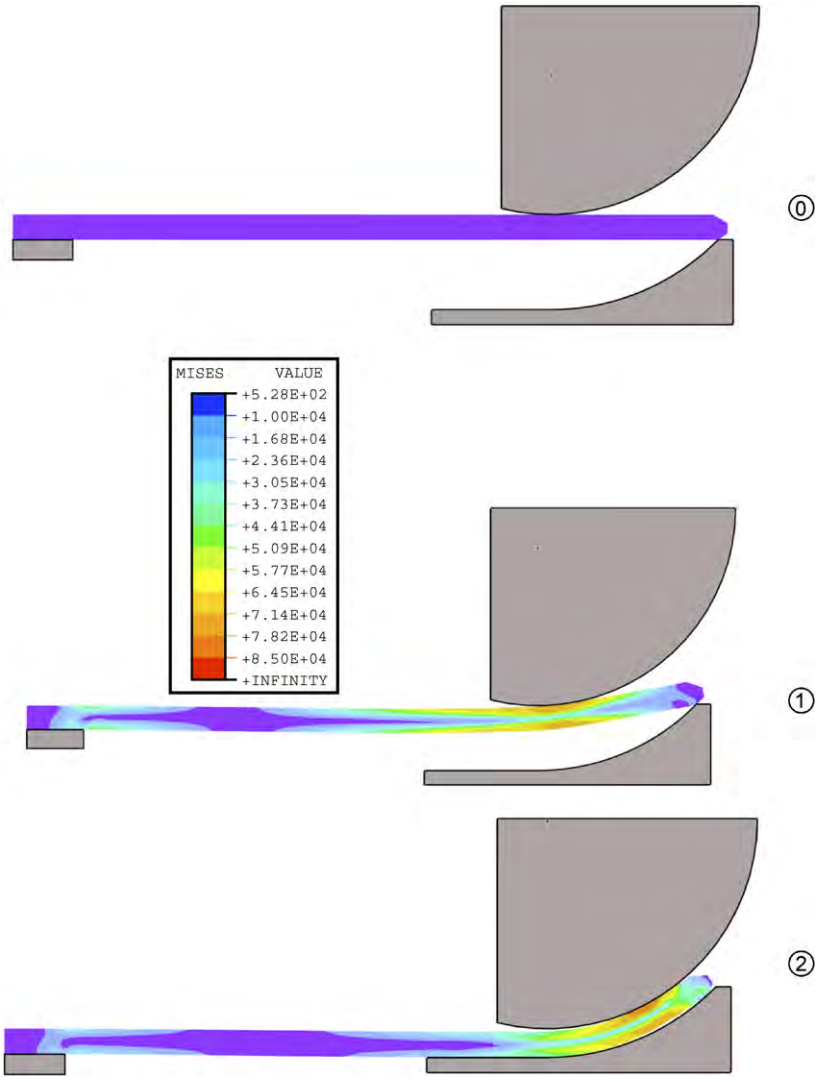

Fig. 7. Three configurations during the crimping process (von Mises stress shown in color contours).

compressed to a strain of $\varepsilon_{C1} = -0.390\%$, and when unloaded, springs back to $\varepsilon_C = -0.171\%$.

4.2. Base case collapse pressure

The collapse pressure is governed by the circularity of the pipe and by the compressive mechanical properties. Fig. 14 shows the shapes of the calculated cross sections of the UO (a), UOE (b) and UOC pipes (c) (with the radial deviation from best-fit circles exaggerated). The shape is affected by each step of the process. Sector A is influenced mostly by the crimp. Sector B corresponds to the straight arms of the skelp. This section is the last to conform to the O-die, and it remains somewhat flatter than the rest of the cross section. Sector C depends on ρ_U, δ_r and ρ_O and is seen to be reasonably circular. Initial ovality is the imperfection that mostly influences collapse under external pressure [2,3]. It is defined as

$$\Delta_o = \frac{D_{\max} - D_{\min}}{D_{\max} + D_{\min}}, \tag{10}$$

where $D_{\max}$ and $D_{\min}$ are the maximum and minimum values of diameter. For the UO pipe, $\Delta_o = 0.848\%$ which is a relatively large value.

Expanding the UO pipe by $\varepsilon_E = 0.984\%$ results in the shape shown in Fig. 14b. The pipe is now much more circular, with $\Delta_o = 0.097\%$. Sector B is still slightly more distorted than the rest of the cross section. The expansion has introduced slight thickness variations in the pipe, as some regions stretched more than others. These are seen greatly distorted in the figure because of the large magnification of w adopted. Concavities introduced by the eight mandrels can be seen on the inner surface. Fig. 14c shows the profile of the actual UOE pipe being simulated. The calculated shape is not exactly the same, primarily because of some differences in the process setting. However the similarity between the two shapes is clearly visible.

Fig. 14d shows the final shape of the UOC pipe in which $\varepsilon_C = -0.171\%$. The shape is somewhat less round than the UOE pipe because of the smaller compressive strain used.

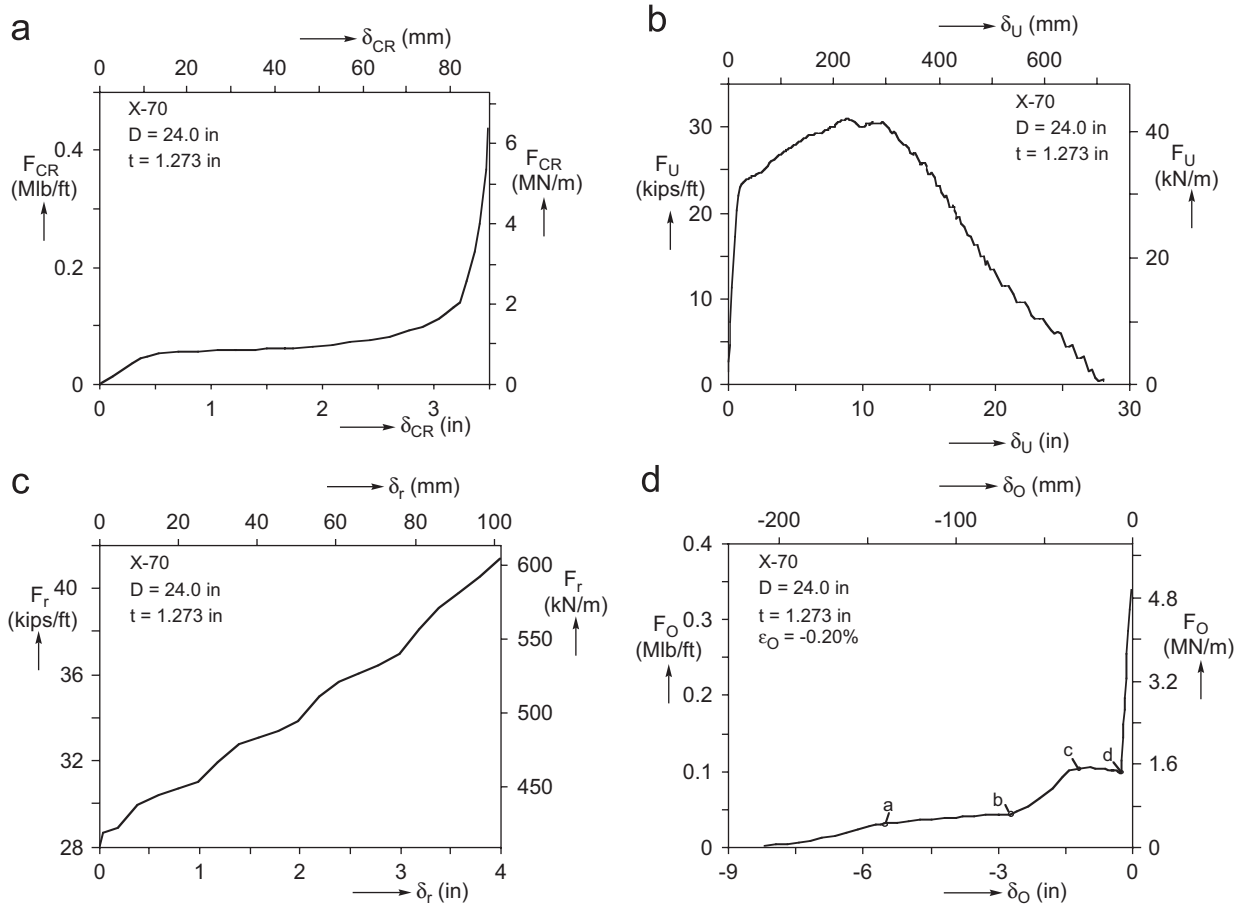

Fig. 8. Force–displacement responses of UOE steps. (a) Crimping, (b) U-punch, (c) U-rollers and (d) O-press.

The ovality in this case is $\Delta_o = 0.192\%$, which is almost double that of the UOE pipe.

In the final step of the simulations, each of the three pipes was pressurized by external pressure. The calculated pressure-change in volume ($P-\delta v$) responses appear in Fig. 15. Each response is initially relatively stiff. At higher pressures, their stiffness is gradually reduced because of inelastic action. Eventually a limit pressure is reached that represents the collapse pressure of the pipe. In an actual experiment, deformation localizes after the pressure maximum as described in Ref. [15]. Localization is of course precluded in the present plane strain solution, but the limit pressure is represented accurately. The collapse pressure of the UO pipe is 4171 psi (287.7 bar) (see Table 3). Note that because of the assumed half symmetry, the pipe must collapse symmetrically, either in a vertical ($\bigcirc$) or in a horizontal ($\bigcirc$) mode. In this case, the pipe collapsed in the vertical mode.

The $P-\delta v$ response of the UOE pipe was overall somewhat stiffer, while the collapse pressure increased to 4895 psi (337.6 bar). In this case, the ovality of the UO pipe was so much larger than that of the UOE pipe that the E-process resulted in a 17.4% increase in collapse pressure. In the next section, it will be demonstrated that this is not always the case.

The $P-\delta v$ response of the UOC pipe was even stiffer and the collapse pressure became 6843 ksi (471.9 bar) and the mode of buckling was horizontal. This particular UOC pipe has nearly double the ovality of the UOE pipe. Despite this it collapses at a pressure that is 40% higher. This confirms the potential benefits of replacing E with C pointed out in Kyriakides et al. (1991) based on results from their 1-D model of the problem.

Finally, a collapse calculation is conducted using the shape of the UOE pipe, assumed to be stress-free, and the monotonic part of the stress–strain response of the plate shown in Fig. 6. This particular combination of geometry and material properties can, for instance, be realized if the UOE pipe is fully heat-treated (normalized). The calculated response included in Fig. 15 stays nearly linear until the limit pressure is reached at 7461 psi (514.6 bar). This value is 52% higher than that of the UOE pipe, illustrating the potential benefits that could be achieved by heat-treating the pipe.

Another evaluation benchmark for the simulation is its capacity to reproduce the changes to the circumferential stress–strain responses introduced by the UOE process. This check was performed as follows. Two integration points near the positions the actual specimens were extracted from (at 180° from weld) were selected, and the

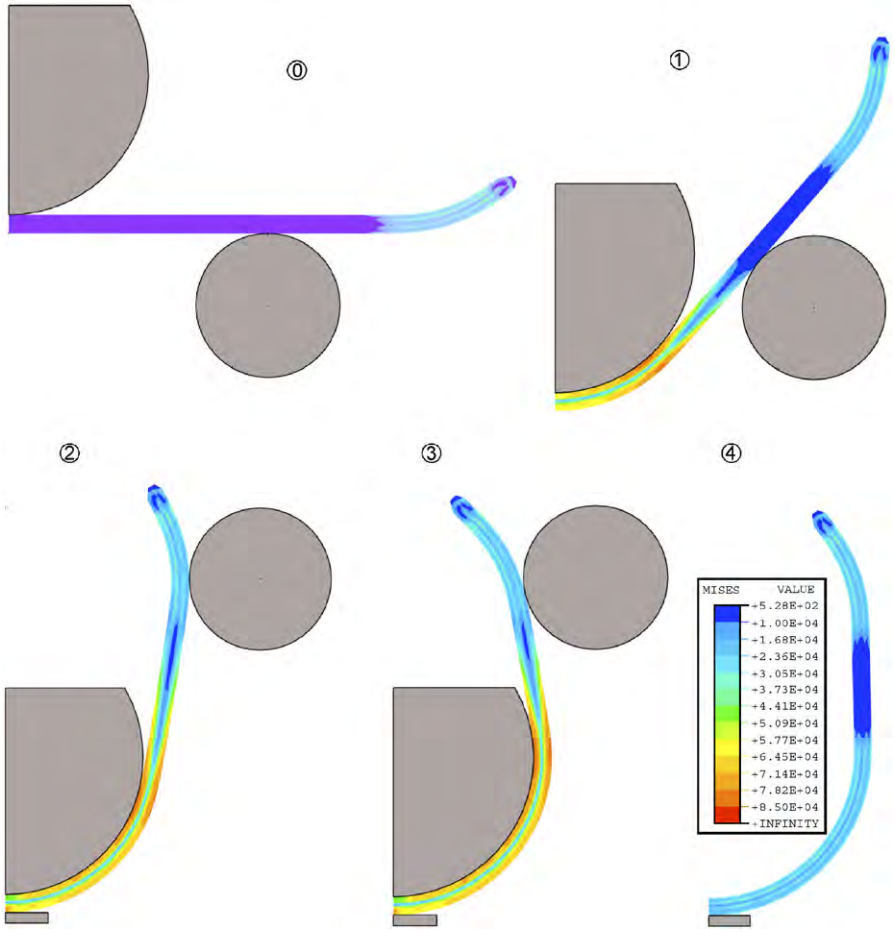

Fig. 9. Sequence of configurations during the U-ing process (von Mises stress shown in color contours).

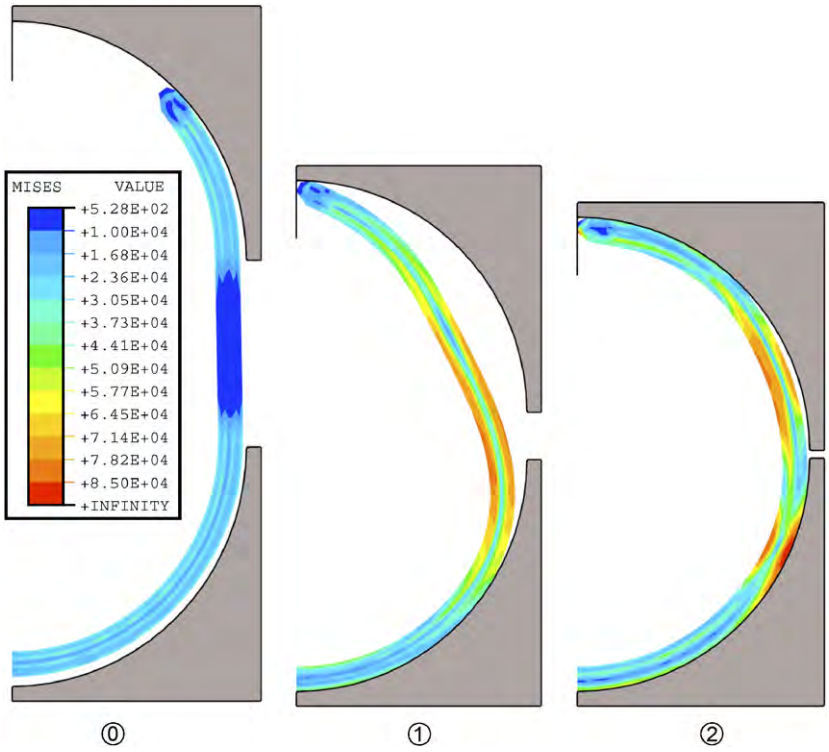

Fig. 10. Initial and two deformed configurations during the O-ing process (color contours show von Mises stress).

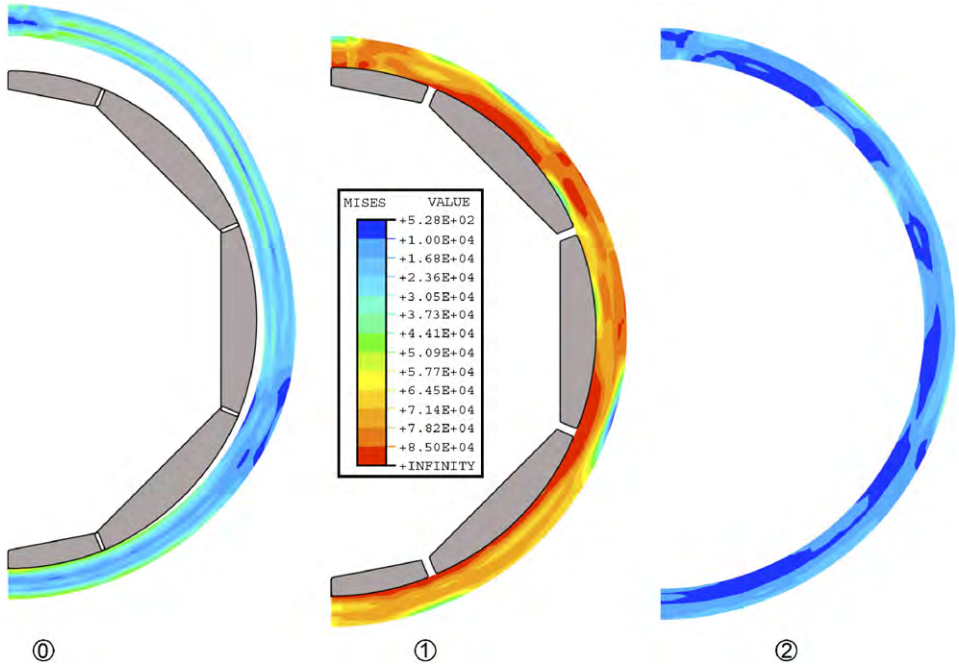

Fig. 11. Three configurations during the Expansion process (von Mises stress shown in color contour).

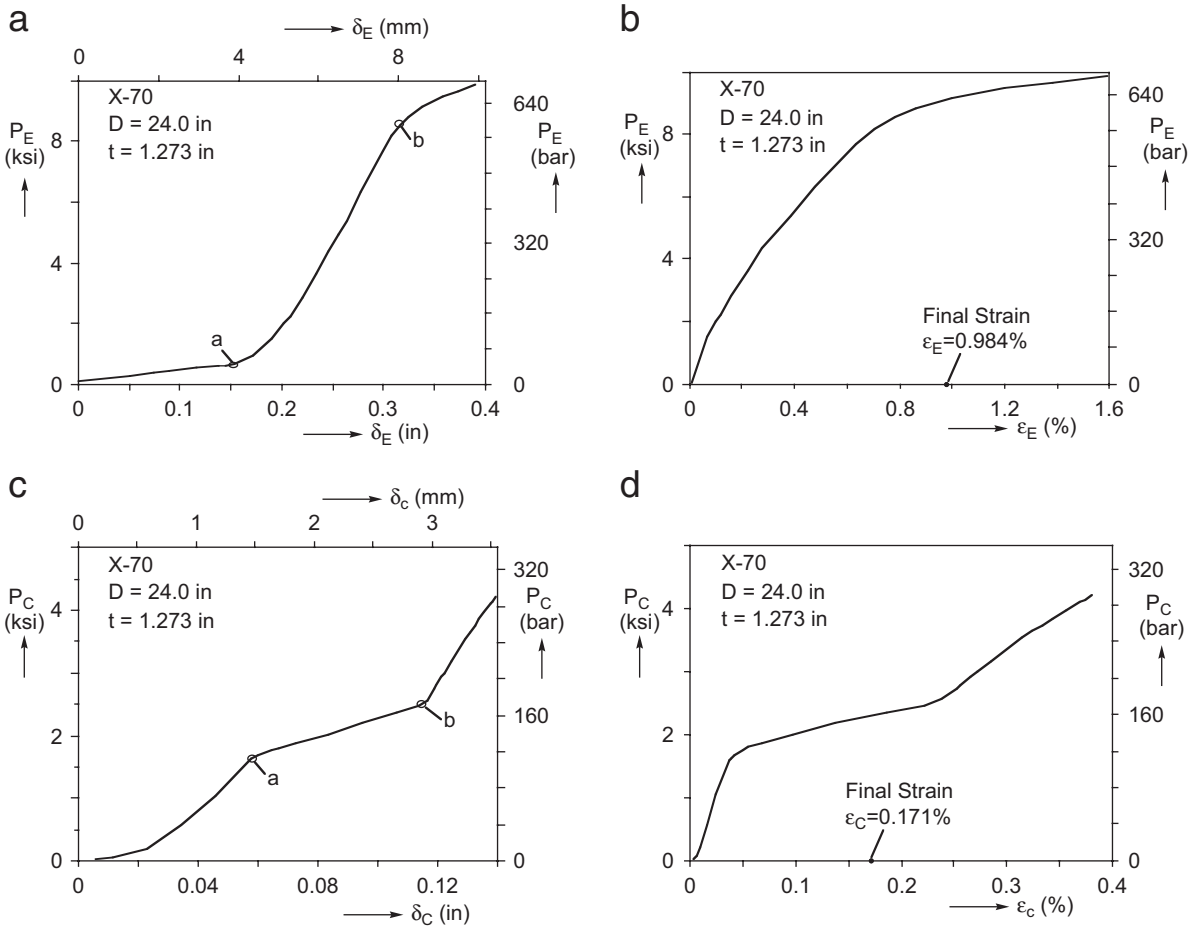

Fig. 12. (a) Pressure–displacement and (b) pressure–strain responses from simulation of expansion. (c) Pressure–displacement and (d) pressure–strain responses from simulation of compression.

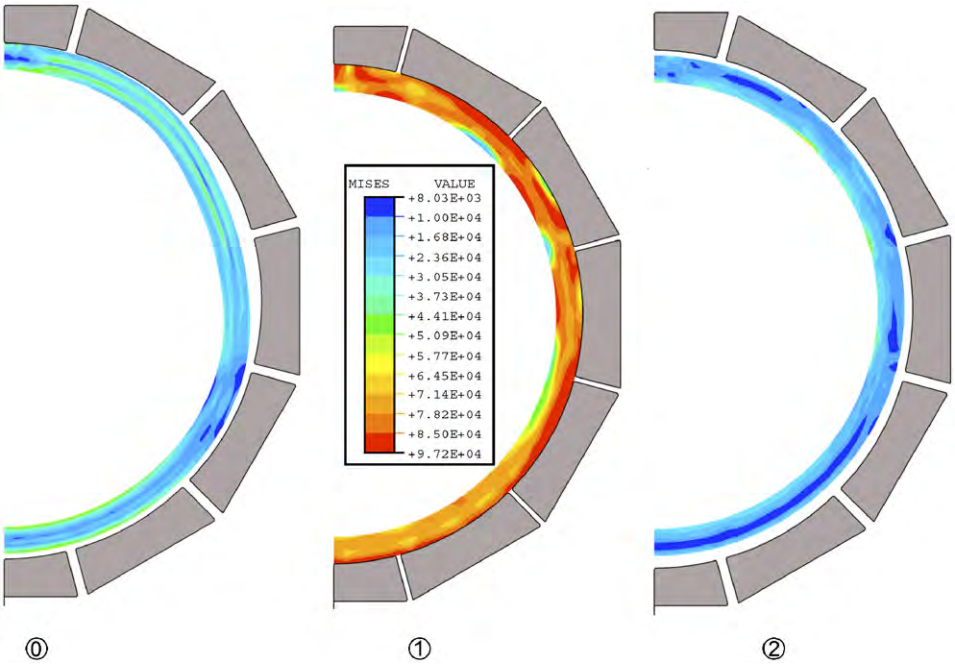

Fig. 13. Three configurations during the compression process (von Mises stress shown in color contours).

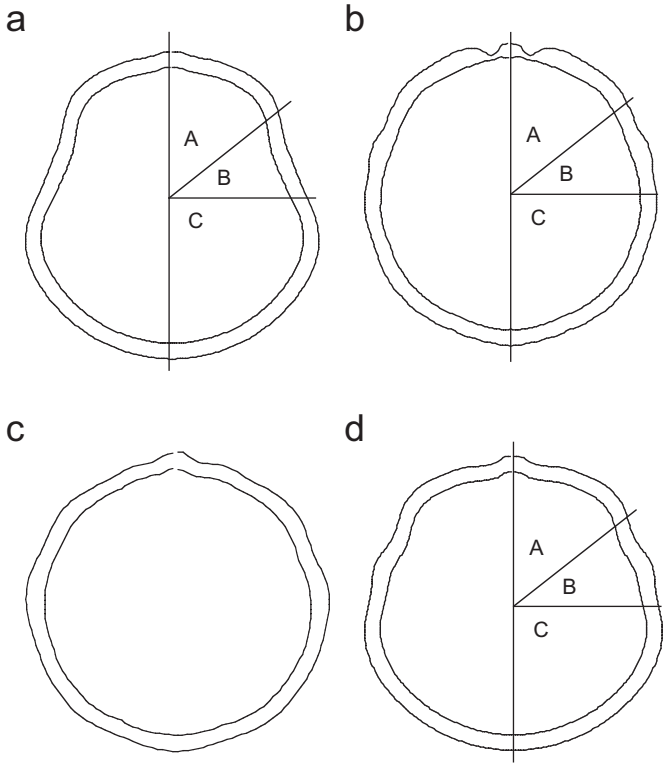

Fig. 14. Pipe cross-sectional shapes from (a) UO simulation, (b) UOE simulation, (c) actual UOE pipe, (d) UOC simulation.

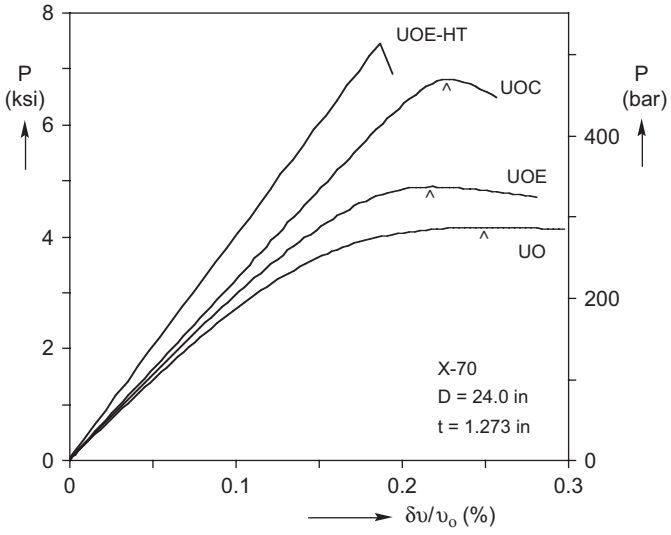

Fig. 15. Calculated pressure-change in volume response of UO, UOE, UOC and "heat-treated" pipe.

state variables locked into these points were recorded. Residual stresses were incrementally reduced to zero, and each point was then loaded to a uniaxial compression strain of 1.0% in the circumferential direction. The predicted stress–strain responses are plotted in Fig. 16. Included are corresponding responses measured experimentally. The comparison is quite favorable.

5. Parametric study of UOE/UOC forming

Each step of the UOE process has variables that influence the shape and collapse performance of the finished pipe. In an effort to quantify the influence of such parameters on pipe performance, several of these variables are varied individually, while keeping all other parameters at the values of the base case (Table 2). Unless otherwise

Table 3
Predicted main pipe shape parameters and collapse pressures

Parameters	UO	UOE	UOC
Circumf. in (mm)	70.855 (1799.7)	71.552 (1817.4)	70.733 (1796.6)
ε (%)	−0.2048	0.9838	−0.1712
Δ_o (%)	0.848	0.0967	0.192
P_{CO} psi (bar)	4171 (287.7)	4895 (337.6)	6843 (471.9)
Mode	0	0	O
P_{CO} HT psi (bar)	—	7461 (514.6)	—

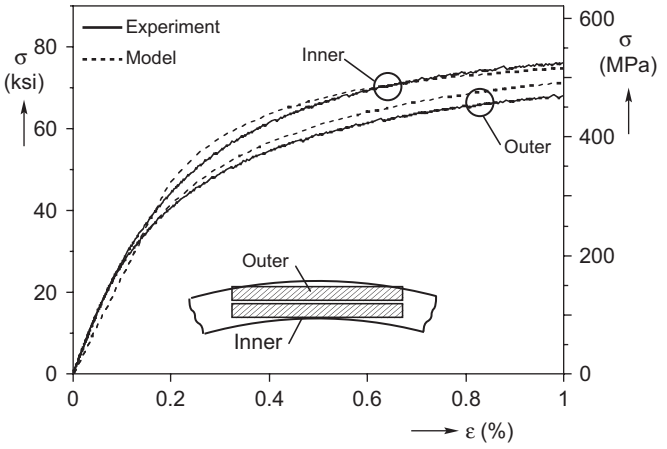

Fig. 16. Comparison of measured and calculated compressive stress–strain responses at two locations through the pipe cross section.

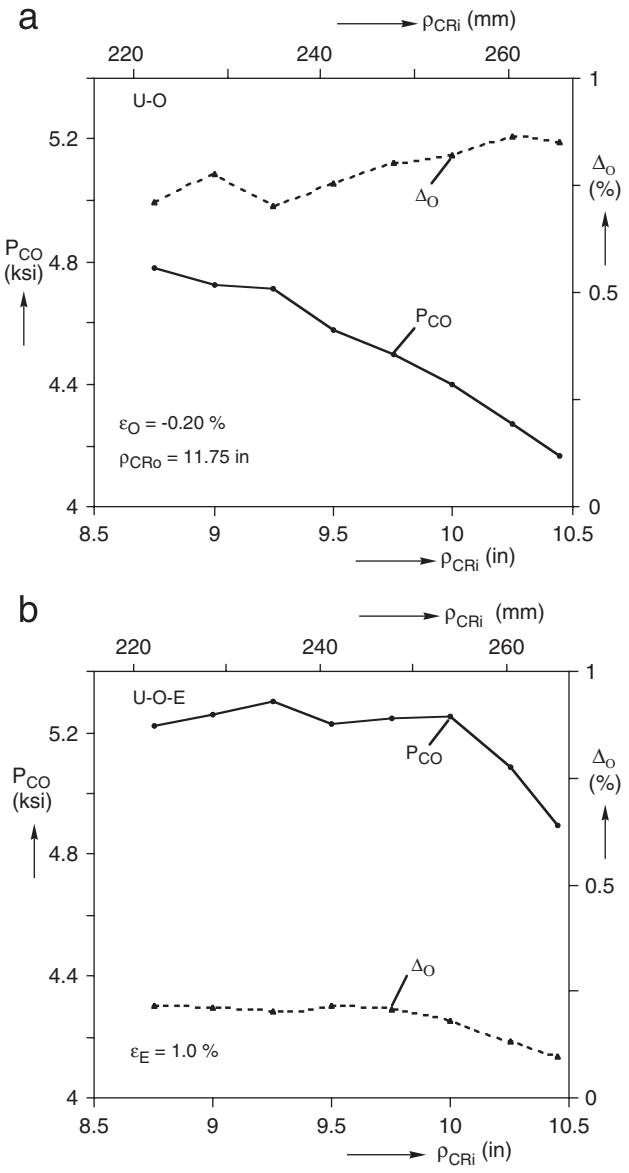

Fig. 17. Effect of ρ_{CRi} on the performance of (a) UO and (b) UOE pipes.

stated, the pipe wall thickness is 1.273 in (32.33 mm) and the O- and E-strains are $\varepsilon_O \approx -0.20\%$ and $\varepsilon_E \approx 1.00\%$. Each pipe is collapsed by external pressure after the UO and again after the UOE (or UOC) steps. Each parameter is varied within a range of values that is considered to be practical. Press load capacities are not considered in these simulations.

5.1. Crimping

The main crimp parameters affecting the pipe shape are the radii of the inner (ρ_{CRi}) and outer radii (ρ_{CRo}), and the length of plate being crimped (L_{CR}). First the radius of the inner crimp die is varied while the radius of the outer die is kept at $\rho_{CRo} = 11.75$ in (298.5 mm). Fig. 17a shows a plot of the ovality and collapse pressure of UO pipe as a function of ρ_{CRi}. The ovality is seen to increase at a low rate nearly linearly with ρ_{CRi}, and as a consequence P_{CO} decreases at a low rate nearly linearly. Thus, a smaller ρ_{CRi} produces a rounder pipe. Collapse calculations are repeated after the pipe is expanded. The ovality and collapse pressure are plotted against ρ_{CRi} in Fig. 17b. Expansion removes most of the out-of-roundness and the collapse pressure increases for all values of ρ_{CRi}. Some degradation in collapse pressure remains for $\rho_{CRi} > 9.75$ in (247.6 mm).

Next, the inner and outer crimping die radii are varied together, with $\rho_{CRo} = (\rho_{CRi} + 1.3)$ in. This strategy ensures that the crimped section has nearly uniform curvature. The variable h_{CR} is kept constant for all the cases, while L_{CR} is adjusted so that the plate edge lines up with the corner of

the outer crimp die. This scheme keeps the length and height of the crimped zones nearly constant, as the radii were varied. Collapse pressures and ovalities are plotted in Fig. 18a for UO pipes and in Fig. 18b for UOE pipes. For both, the highest collapse pressures correspond to the smallest set of radii. As the crimp radii are increased, the collapse pressures drop at first and then steadily rise again. However, overall the collapse pressures are somewhat lower than those in Fig. 17. Again, if the pipe is expanded by 1% the effect of the crimping is essentially erased. When L_{CR} was varied, it was found that increasing its value above that in Table 2 (26.64 in—676.7 mm) produces a modest increase in the UO collapse pressure, but for $L_{CR} > 28$ in (711 mm), the collapse pressure begins to reduce. Again when the pipes are expanded by 1%, the ovality and P_{CO} remain nearly constant with L_{CR}.

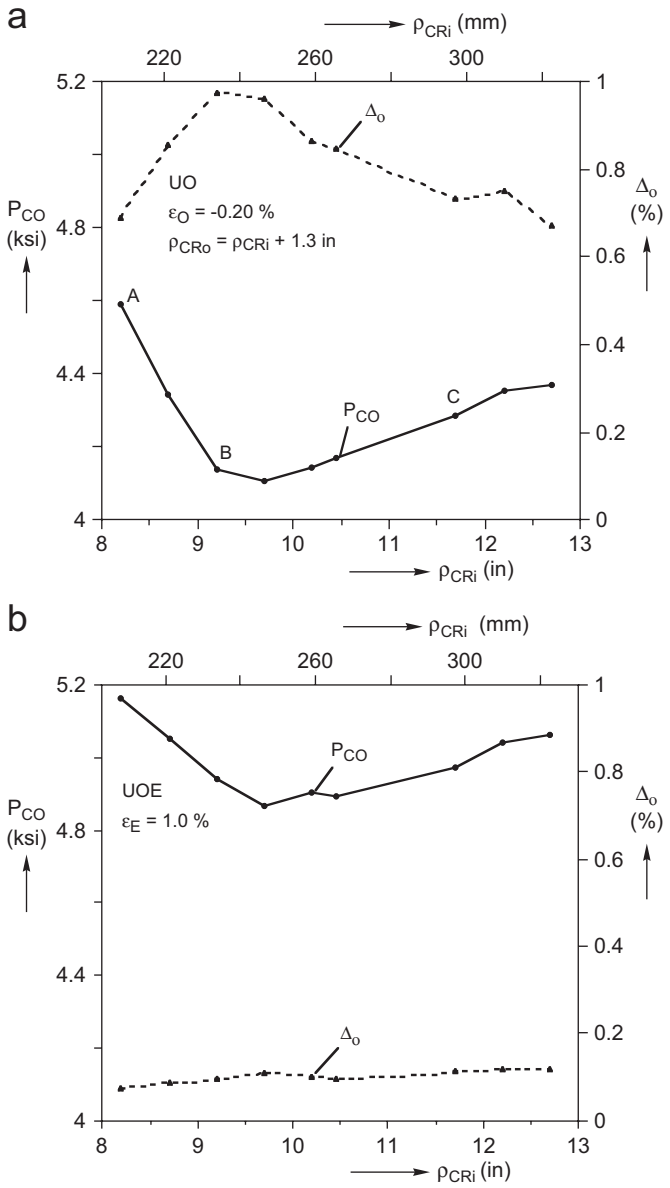

Fig. 18. Effect of ρ_{CRo} and ρ_{CRi} on performance of (a) UO and (b) UOE pipes.

5.2. U-press

The main parameters of the U-press are the distance of the roller center from the plate mid-span (h_r), the vertical displacement (δ_U), the horizontal displacement of the side rollers (δ_r), and the radius of the punch (ρ_U) (Fig. 1b). Each of these was varied and the effect on the collapse pressure of UO and UOE pipes was evaluated. Of these, the only one found to have some effect on P_{CO} is ρ_U. The radius of the U-punch is typically selected to result in a radius of the bottom half of the skelp that is near the desired final radius of the pipe. However, the radius of the skelp must be smaller than the radius of the O-dies for the skelp to fit in the bottom O-die. ρ_U was varied between 8.75 and 10 in (222–254 mm), δ_r is adjusted to produce vertical skelp arms, and all other parameters are kept at the values given in Table 2. The effects of this on the collapse pressure of UO and UOE pipes are shown in Fig. 19a and b, respectively. For the UO pipes, P_{CO} and Δ_o vary approximately linearly with ρ_U, and larger punch radii give significantly rounder and stronger pipes. However, once more, expansion by $\varepsilon_E \approx 1\%$ significantly reduces the magnitude of this effect. It was found that the variation in P_{CO} of UO pipe can be eliminated if in each case the O-dies are moved closer together in order to produce a $\varepsilon_O \approx -0.20\%$. For this to be feasible, the circumference of each half die must be somewhat less than $\pi\rho_O$.

Common practice is to select the roller displacement δ_r so that the skelp arms end up nearly vertical. In this study, δ_r was varied so that the angle between the skelp arms and the vertical varied between -4° and $+10^\circ$ (going below -4° prevents the skelp from fitting inside the top O-die). This has very little affect on the collapse pressure of both UO and UOE pipes.

5.3. O-press

In the O-press, the U-shaped skelp is first bent into a nearly circular shape, and then a net compressive strain ε_O is applied. The radius of the dies (ρ_O) is usually fixed by the diameter of the pipe (standard value). ε_O can be varied by adjusting the displacement of the dies (δ_O), or the width of the plate (W). We first consider varying ε_O by increasing δ_O without concern to die overlap (Fig. 20a) (press load capacity is not considered). As ε_O increases, the collapse pressure goes from just over 3 000 psi (207 bar) at $\varepsilon_O = -0.1\%$ to above 6500 psi (448 bar) $\varepsilon_O = -0.35\%$. It is noted that this increase is partly due to the reduction of the ovality in the pipe seen in the figure, but also due to "hardening" of the material by compression. For $|\varepsilon_O| > 0.35\%$, the collapse pressure starts to decrease somewhat with ε_O. The peak corresponds to the collapse mode switching from vertical ( ) to horizontal orientation ( ). This switch is due to using the closure of the O-dies to vary ε_O.

Fig. 20b shows similar results, in which ε_O is increased by increasing the width of the plate (W). In this process the

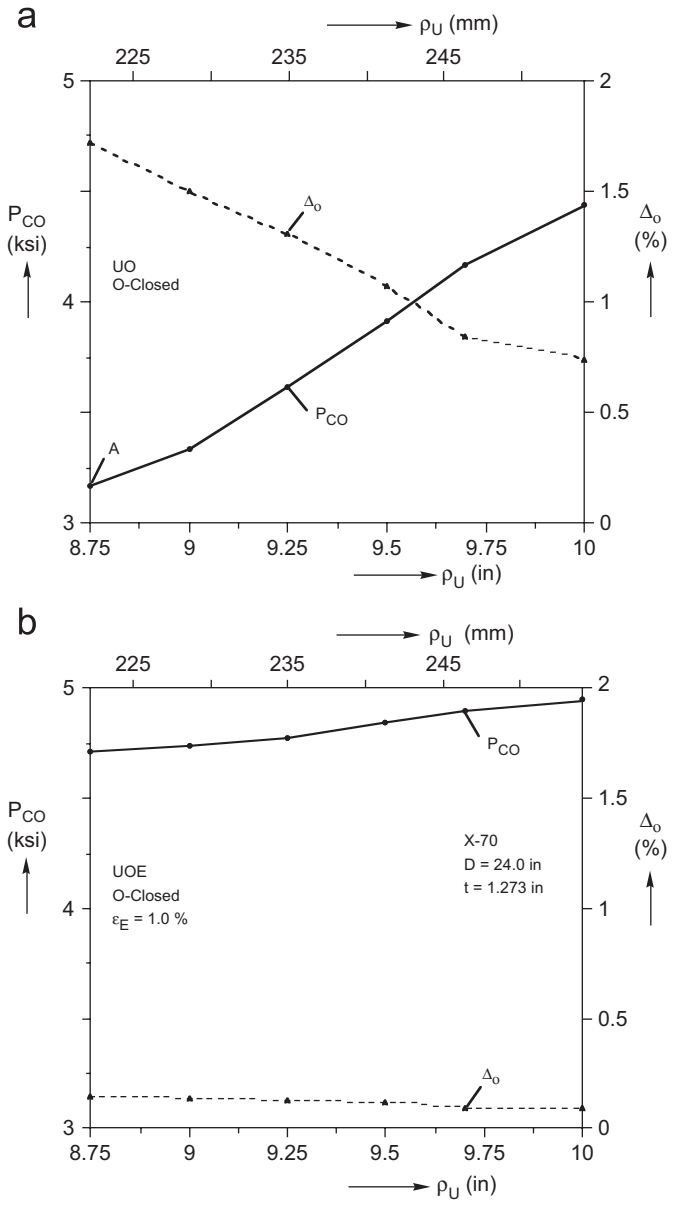

Fig. 19. Effect of ρ_U with fixed δ_O on the performance of (a) UO and (b) UOE pipes.

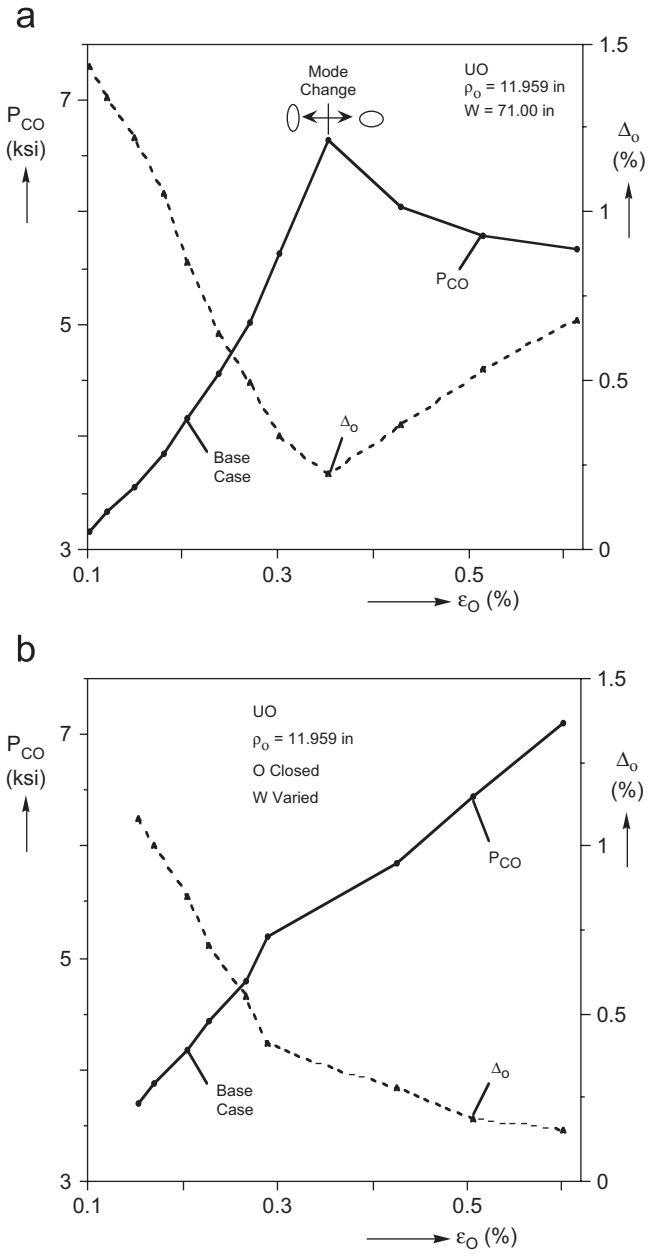

Fig. 20. Effect of ε_O on the performance of UO pipe for (a) δ_O varied and (b) plate width varied.

two halves of the O-press are stopped when they form a perfect circle. As a result, all cases collapsed in the vertical mode and P_{CO} is seen to increase nearly linearly with ε_O. At the highest value of $\varepsilon_O = -0.602\%$ the collapse pressure was over 7 000 psi (483 bar).

5.4. Expansion

Current practice is to expand all UOE pipes by increasing the diameter by about 1% (0.8–1.2%). The effect of ε_E on ovality and collapse pressure on the base case is illustrated in Fig. 21. The starting point ($\varepsilon_E = 0$) is the UO pipe with $\Delta_o = 0.848\%$ and $P_{CO} = 4171$ psi (287.7 bar). As ε_E increases, the ovality initially drops sharply, causing P_{CO} to rise sharply. Further increase in ε_E produces increasingly less improvement in ovality and increasingly more degradation of the compressive material properties. This results in P_{CO} reaching a maximum of 5356 psi (369.4 bar) at $\varepsilon_E = 0.30\%$, with a corresponding ovality of 0.193%. Further increase in ε_O progressively reduces P_{CO}. At $\varepsilon_E = 0.98\%$, the ovality is 0.096% but P_{CO} has dropped to 4895 ksi (337.6 bar).

The same exercise is now repeated for pipes compressed in the O-press to three additional strain values: $\varepsilon_O = 0.269\%$, 0.425%, and 0.506% (achieved by varying the plate width). The pipes are then expanded to different strain levels in the range of 0–1%, and then pressurized to collapse. The final ovality and collapse pressure of these pipes are plotted against ε_E and Fig. 22a and b,

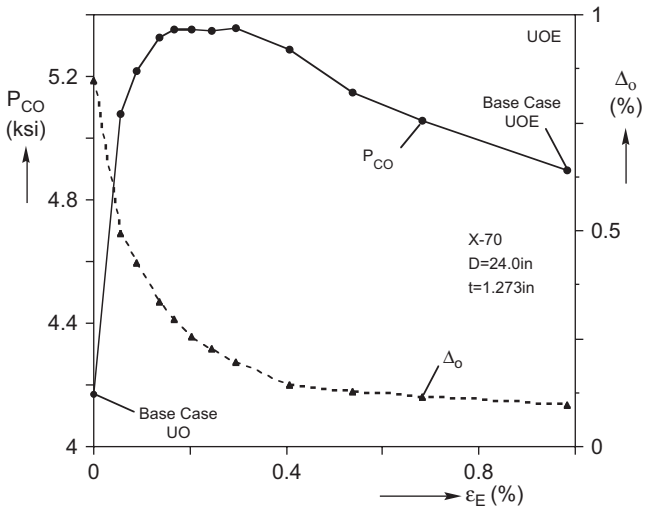

Fig. 21. Effect of expansion on pipe ovality and collapse pressure.

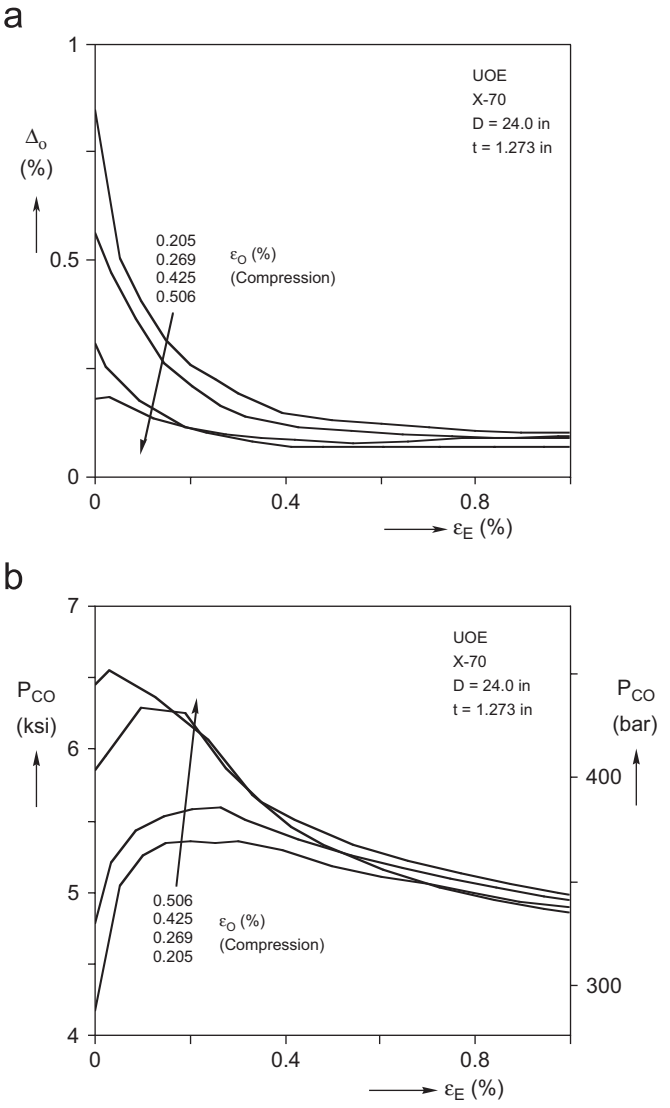

Fig. 22. Effect of ε_E on (a) pipe ovality and (b) collapse pressure for various values of ε_O.

respectively. The cases with $\varepsilon_E = 0$ represent the four pure UO pipes. As ε_O increases, the ovality of the UO pipes decreases with a corresponding increase in collapse pressure. For all cases expansion further reduces the ovality, but most of the benefit occurs for $\varepsilon_E < 0.3\%$. This reduction in ovality has a corresponding positive impact on P_{CO}. However, as was the case for the results in Fig. 21, the positive impact is limited to smaller values of ε_E. Indeed, as ε_O increases, the peak collapse pressure of each case moves to the left, indicating that increasingly less expansion is needed for an optimally performing UOE pipe. At even higher O-strains, the peak collapse pressure corresponds to the UO pipe. Such pipes are already very round and strong, and expansion can only degrade the compressive material strength and lower P_{CO}.

5.5. Compression

The benefits of replacing the Expansion step with Compression are further illustrated in Fig. 23. The base case pipe is formed up to the O-step as before. The pipe is then compressed different amounts (mandrel radius $\rho_C = 11.88$ in—301.8 mm), resulting in net compressive strains (ε_C) ranging from 0% to −0.625%. The calculated pipe ovalities and collapse pressures are plotted vs. ε_C in Fig. 23a and b, respectively. Included in each plot for comparison are the corresponding results from the expanded pipe. Fig. 23a shows that equal amounts of expansion or compression result in pipes with similar ovality levels. At the same time, the collapse pressure of UOC pipe is significantly higher than that of UOE pipe (Fig. 23b). In the case of UOC, P_{CO} first increases nearly linearly with ε_C, reaching a value of 6 843 psi (471.9 bar) at the relatively low $|\varepsilon_C|$ of 0.171%. At this point, the collapse mode changes its orientation from vertical to horizontal, the ovality temporarily rises somewhat, and additional compressive strain is needed until the collapse pressure begins to rise again. Around 0.35% compressive strain, P_{CO} starts increasing again with ε_C reaching a value of 8025 psi (553.4 bar) at $|\varepsilon_C| = 0.625\%$. Indeed, the collapse pressure can increase further if the pipe is compressed to higher values of ε_C. The difference from the corresponding UOE results is very significant. For example, if we compare pipes expanded by 0.625% and contracted by the same amount, UOC has approximately 58% higher collapse pressure.

5.6. Expansion and compression of pipe of various D/t values

The results presented this far are for a pipe with $D/t = 18.85$. We now examine how the expansion and compression strains affect the ovality and collapse pressure of pipes of different D/t values. The material properties used are those in Table 1. The pipe diameter is kept at 24 in

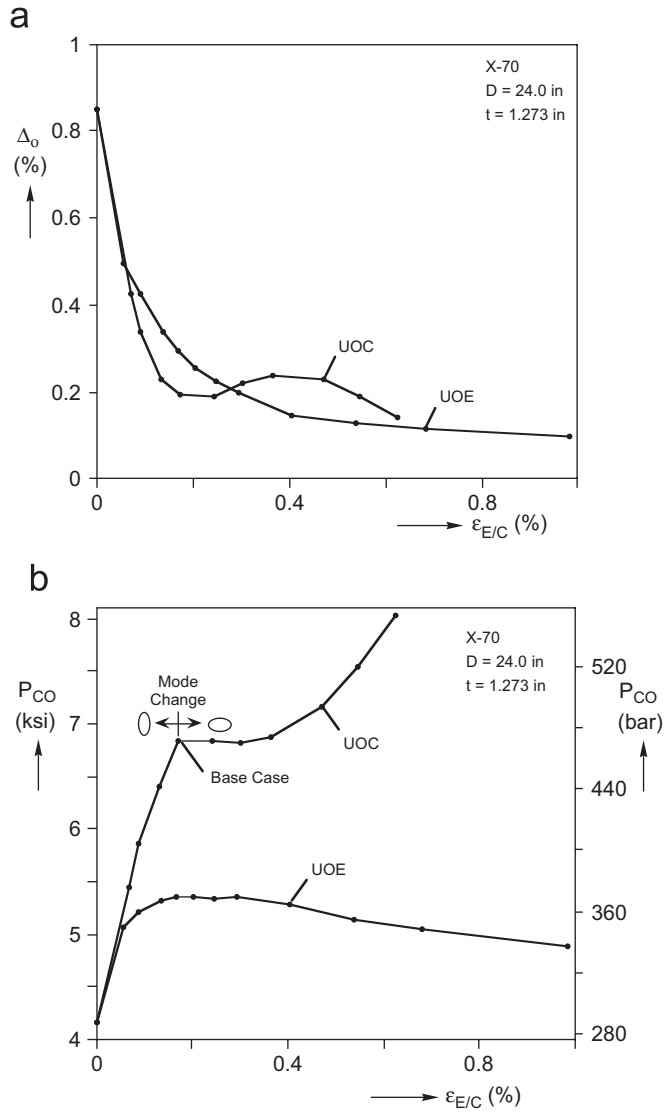

Fig. 23. Effect of ε_E and ε_C (a) pipe ovality and (b) collapse pressure.

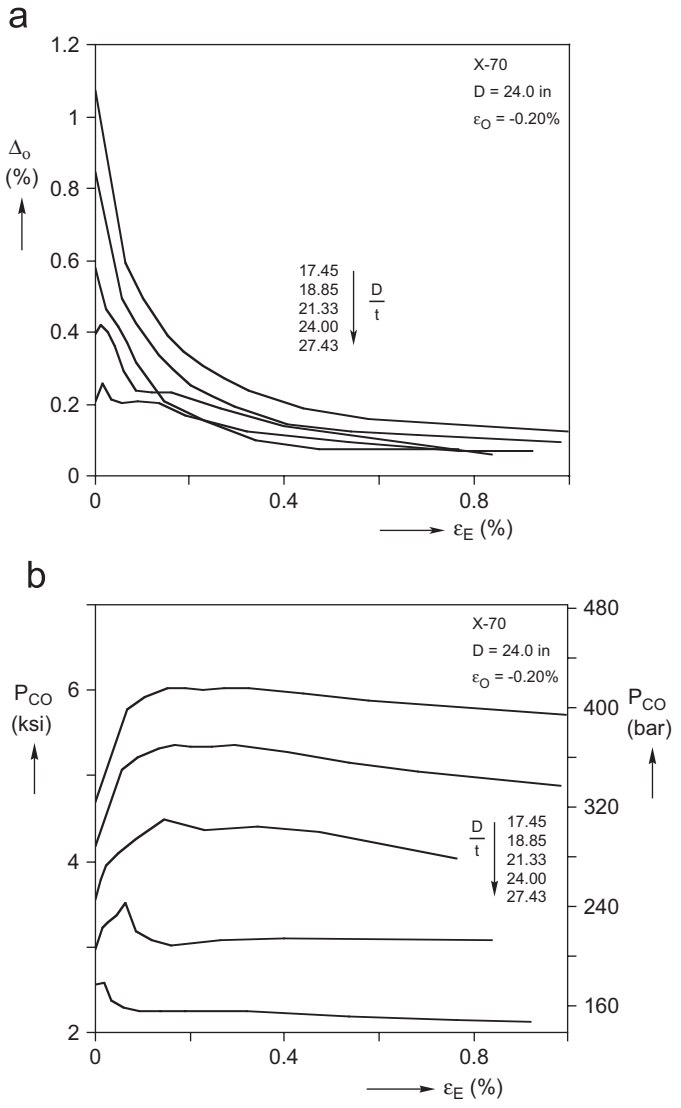

Fig. 24. Effect of ε_E on (a) pipe ovality and (b) collapse pressure for various D/t pipes.

(610 mm), but the thickness is varied to get pipes with the following D/t values: 17.45, 18.85, 21.33, 24.00 and 27.44. In order to optimally form these pipes, the width of the plate (W), the radius of the crimp inner die (ρ_{CRi}), the U-punch radius (ρ_U) and roller displacement (δ_r), and the radius of the expansion mandrels (ρ_E) had to be adjusted. The remaining variables are kept at the levels given in Table 1 (thus $\varepsilon_O = -0.2\%$ for all cases).

Ovality and collapse pressure results are plotted against ε_E for the five D/t values considered in Fig. 24a and b respectively. Expansion has a positive effect on ovality for all D/t values. However, the reduction in ovality is more pronounced at lower D/t values. This is because thinner pipes deformed to the same ε_O have smaller ovality after the O-step. In all cases, most of the reduction in ovality occurs for $\varepsilon_E < 0.35\%$. The collapse pressure of the three thicker pipes is seen to increase with ε_E, reaching a maximum in the neighborhood of 0.3% compression. At higher expansion strains it decreases. For $D/t = 24$, the collapse pressure reaches its maximum at $\varepsilon_E = 0.064\%$. Higher expansions do not improve the collapse pressure above the value of the UO pipe. For $D/t = 27.43$, expanding the pipe to any strain reduces the collapse pressure to a level below that of the UO pipe. In this case the UO pipe has an ovality of only 0.2%. Expansion only moderately reduces the ovality, while simultaneously it degrades in the compressive properties which reduces P_{CO}. In addition, as the D/t increases, the horizontal collapse mode replaces the vertical. For the three thicker pipes ($D/t \leqslant 21.33$), all the cases collapse in the vertical mode. For $D/t = 24.00$, all of the cases right of the peak collapse in the horizontal mode. For $D/t = 27.43$, all of the cases collapsed in the horizontal mode.

A similar set of collapse calculations are performed for the same five D/t pipes as a function of the compressive strain (UOC). Ovality and collapse pressure are plotted

against ε_C in Fig. 25a and b respectively. For the three thicker pipes, finishing the pipe with compression increases the collapse pressure significantly. As D/t increases, the benefit of ε_C is reduced and essentially disappears for the thinnest pipe considered. The sharp local peaks in Fig. 25b correspond to collapse mode changes: cases left of the peak collapse in the vertical mode, while to the right they collapse in the horizontal mode. Fig. 25a reveals that these mode changes correspond to a temporary increase in ovality, and the higher the D/t, the larger the increase. For thinner pipes ($D/t \geqslant 21.33$), this increase in ovality is high enough to cause P_{CO} to drop and give results comparable to the UOE process. As D/t increases, the mode change occurs at increasingly lower compressive strains, until (for $D/t = 27.43$) all of the cases collapse in the horizontal mode. For this pipe, compression is detrimental until relatively high strains ($\varepsilon_C > 0.40\%$) are reached and the ovality is reduced. This trend for higher D/t pipe is, however, similar to what was observed for expanded pipe.

5.7. Effect of material yield stress

In order to examine the effect of yield stress on the process, the basic stress–strain response used is modified to produce the two additional curves shown in Fig. 26a. Keeping all other monotonic response fit parameters the same, the yield stress (σ_{om}) is assigned the values of 76.0 and 61.0 ksi (524 and 490 MPa). In addition, the hysteresis yield stress of the two new curves is adjusted so that $2\sigma_{oc}/\sigma_{om} = 1.55$.

Forming simulations and collapse calculations were performed using the new stress–strain data together with the parameters of the base case given in Table 2. Fig. 26b shows the calculated P_{CO} against σ_{om} for UO, UOE, and UOC pipes. The ovalities are virtually unaffected and therefore are not included. Over this range of yield stress, P_{CO} varies linearly with σ_{om} for all three cold-forming processes and the slope of each curve is nearly identical.

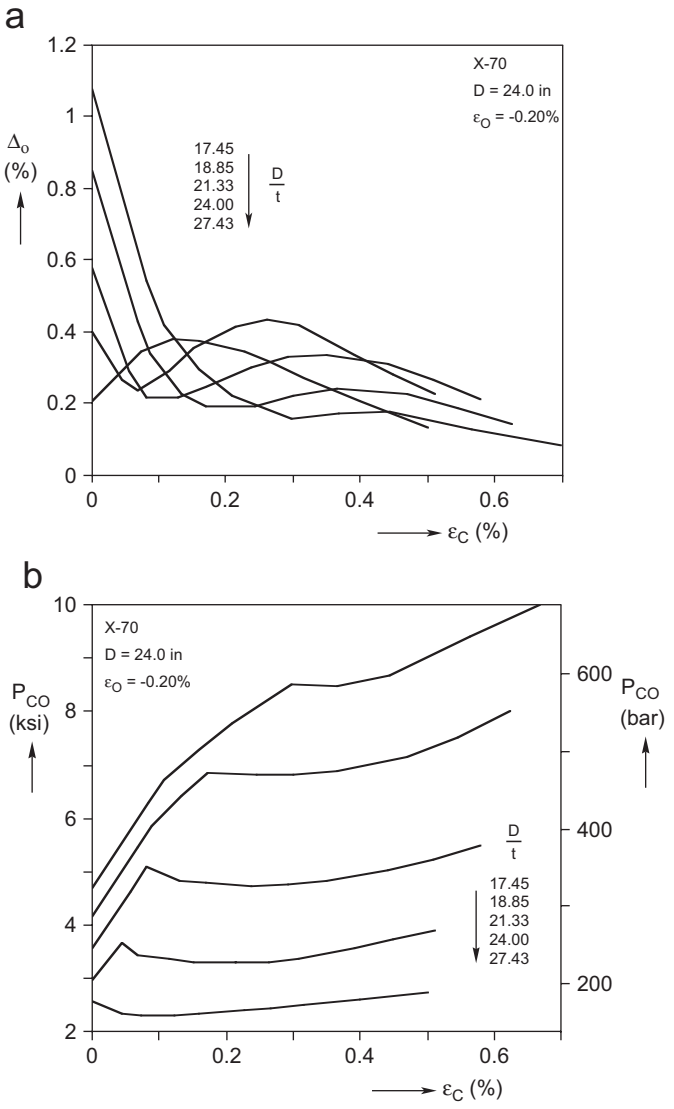

Fig. 25. Effect of ε_C on (a) pipe ovality and (b) collapse pressure for various D/t pipes.

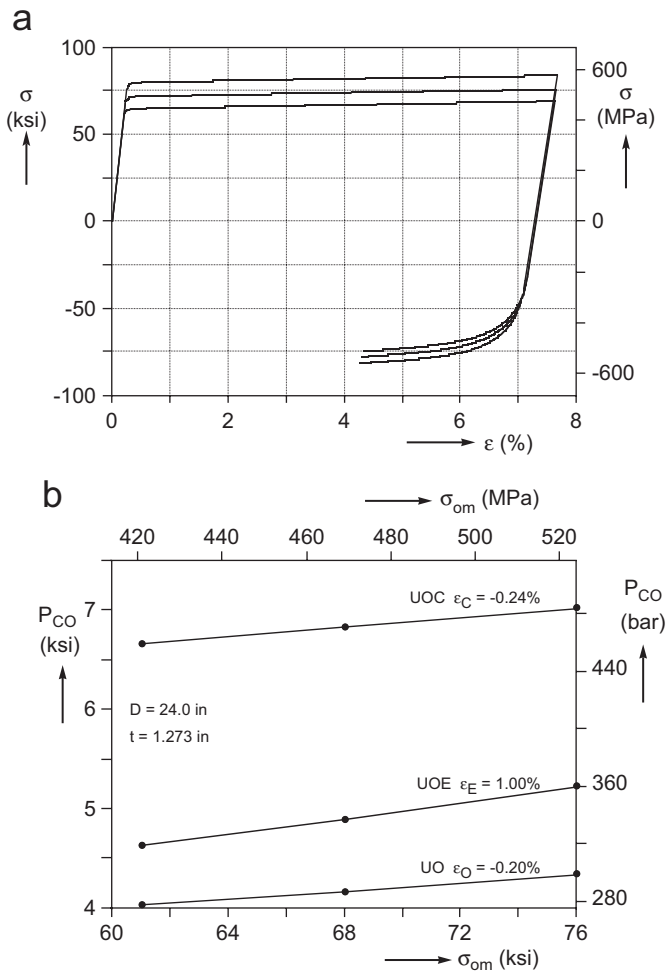

Fig. 26. (a) Three stress–strain responses used in the study. (b) Collapse pressure vs. plate yield stress.

6. Conclusions

The UOE and UOC pipe manufacturing processes have been simulated numerically under plane strain conditions. Following the forming simulation, the pipe was collapsed under external pressure. The capabilities of the numerical scheme where first demonstrated for an X-70 line-grade steel pipe with a diameter of 24 in and wall thickness of 1.273 in (32.33 mm). It was confirmed that the pipe collapse pressure is influenced by its final shape as well as by the mechanical properties in compression. It was shown that the shape produced by the simulation was quite close to that of actual pipes. In addition, it was shown that the model reproduces the degradation in compressive mechanical properties seen in the actual pipe. In this case currently accepted values of compressive strain (-0.2%) in the O-press and expansion strain in the expander (1%) were used. The resulting ovality of UO pipe is relatively high, and thus without the expansion the collapse pressure is rather low. Expansion by 1% reduces the ovality but simultaneously degrades the compressive strength. The net result is that the collapse pressure increased by 17% over that of the UO pipe. When the same pipe was finished with compression, the collapse pressure climbed more than 40% above that of the UOE pipe (depending on the applied ε_C). The possibility of heat-treating the UOE pipe was also investigated by adopting its geometry but assigning the properties of the original plate. In this case the collapse pressure climbed more that 50% above that of the UOE pipe.

In an effort to optimize the forming process for collapse performance, several of the forming parameters were varied individually, and their effect on the collapse pressure of UO and UOE pipe was established. The following conclusions can be drawn from this parametric study.

6.1. Crimping

Crimping affects the shape of the upper part of a UOE pipe. In particular, it affects the shape (and ovality) of UO pipe. It was found that crimp radii (ρ_{CRi} and ρ_{CRo}) that are smaller than the inner and outer radii of the final pipe give higher UO collapse pressures. Furthermore, reducing the length of the crimped part tends to increase the UO collapse pressures. It was also found that if the current practice of expanding the diameter of the pipe by about 1% is followed, both the negative and positive effects of crimping are usually erased. However, if alternate forming solutions such as under expansion are adopted, a more careful selection of the crimping dies can lead to improved collapse performance.

6.2. U-ing

Of the four steps, U-ing affects the UO and UOE collapse pressures the least. The optimal value of ρ_U is the one that produces a pipe radius that closely matches the O-die radius. Its effect is diminished considerably if ε_O of approximately -0.2% is applied and/or an expansion of 1%.

6.3. O-ing

Compression in the O-step is generally beneficial for the collapse pressure of both UO and UOE pipe. The most effective way of increasing ε_O is to increase slightly the initial plate width. For high enough values of ε_O, the collapse pressure is high enough to possibly to avoid expansion altogether (other performance issues not withstanding).

6.4. Expansion

Expansion reduces pipe ovality, but at the same time degrades the compressive mechanical properties. For excessive expansion, this degradation overshadows the improvement in ovality.

The current practice of expanding the pipe by approximately 1% leads to reduced collapse performance for all cases considered. For all cases, the collapse pressure is maximized at expansion strains that are smaller than 0.35%. This happens despite the fact that underexpanded pipes have slightly higher ovality than fully expanded pipes.

For any given UO pipe, an optimum expansion exists that will balance ovality improvement and material degradation effects to maximize P_{CO}. The ε_E that maximizes P_{CO} depends on ε_O; the bigger ε_O applied, the smaller the required ε_E. At higher values of ε_O ($>|0.5\%|$) the UO ovality is quite low, and any expansion may cause reduction in P_{CO} (see results of recent full scale tests in Ref. [16]).

Simulations were conducted for pipes with $17.4 < D/t < 27.5$. In all cases the maximum collapse pressure occurred at values of ε_E less than about 0.3%. The standard practice of expanding to about 1% is too high and detrimental to collapse performance. As D/t increases, the amount of expansion that maximizes P_{CO} decreases. Higher D/t pipes (with $\varepsilon_O \approx -0.2\%$) may not benefit from expansion.

High expansion strains tend to reduce the effect (detrimental or beneficial) on P_{CO} of the parameters of the previous forming steps. The collapse pressure depends mainly on ε_E, and generally decreases as ε_E increases.

6.5. Compression

Compressing a UO pipe instead of expanding it reduces the pipe ovality and increases the pipe's mechanical compressive properties. One way of inducing the required compression is in the O-press. Because the O-press deforms the whole length of the pipe simultaneously, this is limited by press capacity and by other factors. A more attractive alternative is to add a new component to the process, which

will compress the pipe radially in a step-by-step fashion. We envision a segmented female mandrel operating on the outer surface of the pipe (essentially the opposite of the current expansion mandrel) such as the one described in Ref. [11]. The beneficial effects of such a device on the collapse pressure of lower D/t pipes were clearly demonstrated in the simulations. At similar values of strain, UOC yields pipes with similar ovality as UOE but with much higher collapse pressures. High enough compression can increase P_{CO} to values greater than that of the heat-treated pipe, as the material is hardened past the yield stress of the original plate. For example, for the X-70 pipe with $D/t = 18.9$ the collapse pressure of UOE with an expansion of 0.98% is 4895 psi (337.6 bar). If this UOE pipe is fully heat-treated, the collapse pressure can rise to 7461 psi (514.6 bar). The collapse pressure of the UOC pipe is 6843 psi (471.9 bar) for a compression of 0.17%, 8025 psi (553.4 bar) for a compression of 0.625% and even higher values if ε_C reaches 1%.

It is the firm conclusion of this study that the commissioning of a compression device would be an enabling technology for deep-water pipeline applications. What is envisioned is that present expanders will continue to be used for land pipelines, where expansion increases the tensile strength in the hoop direction, and for high D/t offshore pipelines. The compression device would be used for deep-water pipes, where an increase rather than the current reduction in collapse pressure would result in significant savings in materials as well as installation costs. Indeed, for future ultra deep-water applications, the use of the compression device may be the only viable alternative.

Acknowledgments

This work was performed under the JIP Structural Integrity of Offshore Pipelines with financial support from a consortium of industrial sponsors. This support is acknowledged with thanks. The finding, opinions, conclusions and recommendations expressed herein are those of the authors and do not necessarily reflect the views of the sponsors. We wish to also thank Corus Tubes for providing several pipe and plate specimens and for technical support. Special thanks go to David Brereton, Mark Fryer and Peter Tait, for their help and advice over a period of several years on a plethora of details relating to UOE pipe mills.

References

[1] Murphey CE, Langner CG. Ultimate pipe strength under bending, collapse and fatigue. In: Proceedings of the fourth International Conference on Offshore Mechanics and Arctic Engineering 1985;1:467–77.

[2] Yeh M-K, Kyriakides S. On the collapse of inelastic thick-walled tubes under external pressure. ASME Journal of Energy Resources Technology 1986;108:35–47.

[3] Yeh M-K, Kyriakides S. Collapse of deepwater pipelines. ASME Journal of Energy Resources Technology 1988;110:1–11.

[4] Kyriakides S, Corona E, Fischer FJ. On the effect of the UOE manufacturing process on the collapse pressure of long tubes. In: Proceedings of the Offshore Technology Conference, OTC6758 1992;4:531–43;
Kyriakides S, Corona E, Fischer FJ. On the effect of the UOE manufacturing process on the collapse pressure of long tubes. ASME Journal of Engineering for Industry 1994;116:93–100.

[5] Stark PR, McKeehan DS. Hydrostatic collapse research in support of the Oman–India gas pipeline. In: Proceedings of the Offshore Technology Conference, OTC7705 1995;2:105–20.

[6] Al-Sharif AM, Preston R. Improvements in UOE pipe collapse resistance by thermal aging. In: Proceeding of the Offshore Technology Conference, OTC8211 1996;2:579–88.

[7] Hall EO. Yieldings of the point phenomena in metals and alloys. New York: Plenum Press; 1970.

[8] DeGeer D, Marewski U, Hillenbrand H-G, Weber B, Crawford M. Collapse testing of thermally treated line pipe for ultra-deepwater applications. In: Proceedings of the 24th International Conference on Offshore Mechanics and Arctic Engineering, June 20–25, Vancouver, BC, Canada, Paper OMAE2004-51569, 2004.

[9] DeGeer D, Timms C, Lobanov V. Blue stream collapse test program. In: International Conference on Offshore Mechanics and Arctic Engineering, June 12–17, Halkidiki, Greece, Paper OMAE2005-67260, 2005.

[10] Shinohara Y, Hara T, Tsuru E, Asahi H, Tereda Y, Doi N. Change of mechanical properties of high strength line pipe by thermal coating treatment. In: International Conference Offshore Mechanics and Arctic Engineering, June 12–17, Halkidiki, Greece, Paper OMAE2005-67055, 2005.

[11] Ewart JC. Apparatus for radially compressing articles. US Patent 2,999,405, A.O. Smith Corporation, 1961.

[12] Dafalias YF, Popov EP. A Model of nonlinearly hardening materials for complex loading. Acta Mechanica 1975;21:173–92.

[13] Dafalias YF, Popov EP. Plastic internal variables formalism of cyclic plasticity. ASME Journal of Applied Mechanics 1976;43:645–51.

[14] Mroz Z. On the description of anisotropic workhardening. Journal of Mechanics and Physics of Solids 1967;15:163–75.

[15] Dyau JY, Kyriakides S. On the localization and collapse in cylindrical shells under external pressure. International Journal of Solids and Structures 1993;30:463–82.

[16] Fryer M, Tait P, Kyriakides S, Timms C, DeGeer D. The prediction and enhancement of UOE-DSAW collapse resistance for deepwater pipelines. In: Proceedings of the fifth biennial International Pipeline Conference, October 4–8, 2004, Calgary, AL, Canada, vol. 3, p. 1961–6.